SUPERCONDUCTIVITY IN METAL-SEMICONDUCTOR EUTECTIC ALLOYS

Thesis by

William L. Johnson

In Partial Fulfillment of the Requirements

For the Degree of

Doctor of Philosophy

California Institute of Technology

Pasadena, California

1975

(Submitted August 1974)

To My Parents

ACKNOWLEDGMENT

The author wishes to acknowledge Dr. C. C. Tsuei who worked jointly with him in much of this work. Dr. Tsuei's friendship and inspiration have been invaluable. The continuous support, advice and encouragement given by Professor Pol Duwez are gratefully acknowledged. The author thanks Sumio Kotake, Concetto Geremia, Frank Youngkin, and Joe Wysocki for technical assistance, and Angela Bressan and Bonita Coates for typing the manuscript. The financial support of the U.S. Atomic Energy Commission has made this research possible.

ABSTRACT

The superconductivity of several metal-semiconductor simple eutectic alloys containing Ge or Si, and one of the metals Al, Be, In, Pb, Sn, or Tl has been investigated. The liquid-quenching technique was used to reduce the characteristic scale of the microstructure in the alloys. It was found in some cases (notably Al-base alloys) that the superconducting transition temperature of the metallic phase was significantly enhanced (from $1.2^{o}K$ to $\sim 6^{o}K$ for Al-base alloys) as a result of liquid-quenching. The characteristic scale of the microstructure was found to be of the order of several hundred angstroms in alloys showing the greatest enhancement effect. The results are discussed in terms of recent theoretical models that predict enhancement of superconductivity due to electronic interactions at a metal-semiconductor interface. The results are also analyzed in terms of the McMillan theory of superconductivity in which the enhancement effect is attributed to a reduction in the characteristic phonon frequencies of the metal. It is concluded that the latter explanation can account for all of the observed properties and, thus, that it is probably unnecessary to invoke an "excitonic mechanism" to explain the results.

TABLE OF CONTENTS

		Page
I.	INTRODUCTION	1
II.	EXPERIMENTAL PROCEDURES	7
III.	RESULTS	11
	A. As-Cast Aluminum Alloys	11
	1. Microstructure and x-stal structure	11
	2. Electrical resistivity	13
	3. Magnetic measurements	17
	B. Liquid-Quenched Aluminum Alloys	26
	1. Crystal structure and microstructure	26
	2. Electrical resistivity	30
	3. Magnetic measurements	33
	4. Annealing behavior	37
	C. Results for Other Alloys	37
IV.	ANALYSIS AND DISCUSSION	48
	A. Enhancement of Superconducting Transition Temperatures	48
	B. Magnetic Properties	71
	C. Size Effects	81
V.	SUMMARY AND CONCLUSIONS	83
REFERENCES		87

LIST OF TABLES

		Page
TABLE I.	Composition of the Alloys Studied	8
TABLE II.	Summary of X-ray Analysis Results and Superconducting Transition Temperatures (Determined From Electrical Resistivity) for As-cast Alloys .	12
TABLE III.	Summary of Results of X-ray Analysis and Superconducting Transition Temperature (From Electrical Resistivity) for Liquid-Quenched Alloys .	22
TABLE IV.	Superconducting Transition Temperatures of Pure Metals	39
TABLE V.	Predicted Values of T_c Using McMillan Approach for an f.c.c. Solid Solution of Si in Al With $\lambda_{Al} = 0.30$ and $\lambda_{Al} = 0.38$ Compared to Observed Transition Temperatures of Al-Si Alloys. It Is Assumed that the Si Content of the Solid Can Not Exceed 11 at.%	57
TABLE VI.	Approximate Values for λ_{ex}, b, t_{Al}, and D for a Given Al Transition Temperature T_c. Values of $\gamma \sim 1/3$, $S \sim 1/3$, $\hbar\omega_p = 10eV$, $\hbar\omega_g = 1eV$, and $\mu = 0.3$ Were Assumed.	69
TABLE VII.	Summary of Parameters Characterizing the Magnetic Properties of As-cast $Al_{70}Ge_{30}$ and Liquid-Quenched $Al_{70}Si_{30}$. The Temperature is Taken to be 1.3^oK for Temperature Dependent Parameters . .	79

LIST OF FIGURES

		Page
FIGURE 1.	Phase Diagram of Al-Si (From Ref. 9)	4
FIGURE 2.	Scanning Electron Micrographs of (a) As-cast $Al_{70}Ge_{30}$, (b) As-cast $Al_{70}Ge_{30}$ Annealed at 400°C for 1 Day; and Metallographs of (c) As-cast $Al_{70}Si_{30}$, and (d) As-cast $Al_{82}Cu_{18}$.	14
FIGURE 3.	Scanning Electron Micrograph of Liquid-Quenched $Al_{70}Si_{30}$ Showing a Region Near the Copper Substrate.	15
FIGURE 4.	Electrical Resistivity as a Function of Temperature for As-cast $Al_{70}Ge_{30}$, $Al_{70}Si_{30}$, And $Al_{70}Ge_{30}$ Annealed at 400°C for 1 Day. . . .	16
FIGURE 5.	Longitudinal Magneto Resistance at 1.3°K for $Al_{70}Ge_{30}$ As-cast. The Insert Shows the Low Field Behavior.	18
FIGURE 6.	Longitudinal Magneto Resistance at 1.3°K for $Al_{70}Si_{30}$ As-cast. The Insert Shows the Low Field Behavior.	19
FIGURE 7.	Critical Current J_c at 1.3°K as a Function of Magnetic Field for (a) As-cast $Al_{70}Si_{30}$ and (b) As-cast $Al_{70}Ge_{30}$.	20
FIGURE 8.	Electrical Resistivity as a Function of Temperature for Al_5Ge_{95} (Right Hand Scale in Ωcm) and $Al_{50}Si_{50}$ (Left Hand Scale in 10^{-4} Ωcm) As-cast.	21

LIST OF FIGURES Continued

Page

FIGURE 9. Relative Inductance Change as a Function of Temperature for As-cast $Al_{70}Ge_{30}$ and $Al_{70}Si_{30}$. 25

FIGURE 10. Magnetization as a Function of Magnetic Field for As-cast $Al_{70}Ge_{30}$. 27

FIGURE 11. Lattice Parameter of the Al Phase in Liquid-Quenched Al-Si Alloys as a Function of Si Content. 28

FIGURE 12. Electrical Resistance Ratio (R/R_0) (R_0 is the Residual Resistance at 8^oK) as a Function of Temperature for (a) $Al_{95}Si_5$, (b) $Al_{70}Si_{30}$, (c) $Al_{60}Si_{40}$ All Quenched from the Liquid State. 31

FIGURE 13. Superconducting Transition Temperature as a Function of Composition for Liquid-Quenched Al-Si Alloys. 32

FIGURE 14. Longitudinal Magnetoresistance at 1.3^oK as a Function of Magnetic Field for Liquid-Quenched $Al_{70}Si_{30}$. 34

FIGURE 15. Relative Inductance Change as a Function of Temperature for Two Samples of Liquid-Quenched $Al_{70}Si_{30}$. 35

FIGURE 16. Magnetization as a Function of Magnetic Field at $T = 1.4^oK$ for $Al_{70}Si_{30}$ Quenched from the Liquid State. Arrows Indicate Direction of Field Change. 36

FIGURE 17. Electrical Resistance Ratio (R/R_0) (R_0 = Resistance at 10^oK) as a Function of Temperature for (a) Liquid-Quenched $Sn_{20}Ge_{80}$, and (b) Liquid-Quenched $Sn_{70}Ge_{30}$. 40

LIST OF FIGURES Continued

Page

FIGURE 18. Relative Inductance Change as a Function of Temperature for (a) Liquid-Quenched Sn, and (b) Liquid-Quenched $Sn_{20}Ge_{80}$. 41

FIGURE 19. Relative Inductance Change as a Function of Temperature for (a) As-cast $Ga_{10}Ge_{90}$, and (b) Liquid-Quenched $Ga_{10}Ge_{90}$. 42

FIGURE 20. Electrical Resistance Ratio (R/R_o) (R_o = Residual Resistivity at 10^oK) as a Function of Temperature for (a) Liquid-Quenched $Ga_{50}Ge_{50}$, and (b) Liquid-Quenched $Ga_{10}Ge_{90}$. 43

FIGURE 21. Electrical Resistance Ratio (R/R_o) (R_o = Residual Resistance at 10^oK) as a Function of Temperature for (a) Liquid-Quenched $Be_{25}Si_{75}$, and (b) Liquid-Quenched $Be_{45}Si_{55}$. 45

FIGURE 22. Electrical Resistance Ratio (R/R_o) (R_o = Residual Resistance at 10^oK) as a Function of Temperature for (a) Liquid-Quenched $In_{70}Ge_{30}$, and (b) Liquid-Quenched $Pb_{70}Ge_{30}$. 47

FIGURE 23. Maximum Observed Enhancement of T_{c0} (Bulk Metal Transition Temperature) as a Function of Fermi Energy Calculated from Free Electron Model for Various Metals in this Study. 64

FIGURE 24. Illustration of the Metal-Semiconductor Domain Geometry Used in Applying the ABB Model. In the Diagram, M Refers to the Metal (Al) Domain and S to the Semiconducting (Si) Domain. 65

LIST OF FIGURES Continued

Page

FIGURE 25. The Dependence of the Superconducting Transition Temperature of an Al Domain on the Exciton Coupling Strength λ^*_{ex} Calculated from the ABB Model. 67

FIGURE 26. Example of Results of Numerical Calculations by ABB Showing the Predicted Dependence of T_c on the Fermi Energy of the Metal. In the Figure, A is the Width of the Exciton Spectrum, and μ is the Coulomb Coupling Constant. . . . 72

FIGURE 27. Illustration of the Model of a Lamellar Colony Used in Calculating the Magnetic Properties of As-cast $Al_{70}Ge_{30}$. 73

I. INTRODUCTION

Superconductivity in metal-dielectric systems is a subject of much current interest. Various mechanisms leading to superconductivity as a result of an interface interaction in such binary systems have been suggested. (References 1-5.) Some theoretical predictions indicate that under favorable conditions higher superconducting transition temperatures might be expected from such systems than can be achieved with the conventional BCS type of phonon mechanism alone. This theoretical work has spurred several experimental efforts devoted to demonstrating the existence of the suggested mechanisms. (References 6, 7, and 8.) Most of the experimental work has been confined to studies of thin films obtained by vapor deposition. Ultrathin metal layers on semiconducting or insulating substrates, covapordeposited metal-dielectric mixtures, and alternating metal-dielectric layered sandwiches have been given much attention; however, the problems and uncertainties which accompany the study of vapor deposited films have caused much confusion and controversy over the interpretation of experimental results.

In an eutectic alloy, obtained by melting the constituents, alternating domains of metal and dielectric phases can exist in a microscopic array. The scale of the microstructure is known to depend sensitively on the rate of cooling from the melt, providing a natural means of varying the typical domain sizes in such a binary system. Using rapid cooling techniques, one might expect to achieve

extremely small interspersed domains of metal and dielectric. In this fashion, many of the uncertainties arising in vapor deposition experiments can be eliminated. In particular, gaseous contamination and the problem of achieving intimate contact between layers can be significantly reduced. Also, the larger sample size facilitates the measurement of such bulk properties as magnetic susceptibility. Of course, new uncertainties may be introduced; however, this approach to the problem of superconductivity in a metal-dielectric systems is interesting enough to warrant systematic investigation and provided the motivation for the present study. Simultaneous studies of microstructure, x-stal structure, and superconducting properties of several metal-dielectric eutectic alloy systems have been carried out with the aim of evaluating the possible role of an interface interaction in the superconductivity of these alloys.

Several important points were considered in selecting appropriate alloy systems for the investigation. To begin, the alloys should ideally consist of two separate, well-defined phases, one of which has metallic properties and the other either semiconducting or insulating properties. The choice of simple eutectic alloys guarantees the exclusive presence of two distinct phases in thermodynamic equilibrium; however, only Si and Ge taken together with a limited number of metals are found to have this type of equilibrium phase diagram. Other semiconductors like Te and Se are found invariably to form intermediate crystalline phases with metals and are thus generally unacceptable for this study. It should be mentioned, however, that distinct metallic and semiconducting phases might be obtained in more complex

systems. For example, binary alloys of Pb and Te of the form Pb_xTe_{100-x} with $x > 50$ could be used. (Reference 9.) The single intermediate PbTe phase coexists with a Pb phase in such Pb-rich alloys.

The simple eutectic phase diagram of Al-Si is shown in Figure 1 to illustrate its general features. (Reference 9.) The eutectic composition occurs at 11.3 at.% of Si. At this composition, the alloy is completely liquid above 577°C and solid below this temperature. Solid Al dissolves a maximum of $\sim$ 1.6 at.% Si at 577°C, and the solubility falls to less than 0.1 at.% of Si at room temperature. Al is nearly insoluble in solid Si. The mutual solubility of the metal and semiconducting phases is of extreme importance in the present study since the electronic properties of a semiconductor are extremely sensitive to metallic impurities. Likewise, dissolved Si or Ge in the metallic phase of the alloy can influence both electronic and lattice properties of the metal and in turn its superconducting properties. Ideally, the two phases should be mutually insoluble. This condition is unfortunately not respected in most cases. Typically, for simple eutectic alloys (e.g., Al-Si, Al-Ge, Sn-Ge, etc.) the metal is nearly insoluble in the semiconducting phase, whereas a limited solubility of Ge or Si is observed in the metallic phase. More complex systems (e.g., Pb-Te) containing a semiconducting compound tend to exhibit a larger solubility of the metal in the semiconducting phase as illustrated by the large homogeneity range for formation of the compound PbTe. (Reference 9.) This has a catastrophic effect on the electronic properties of the semiconductor. In the case of PbTe, it results in

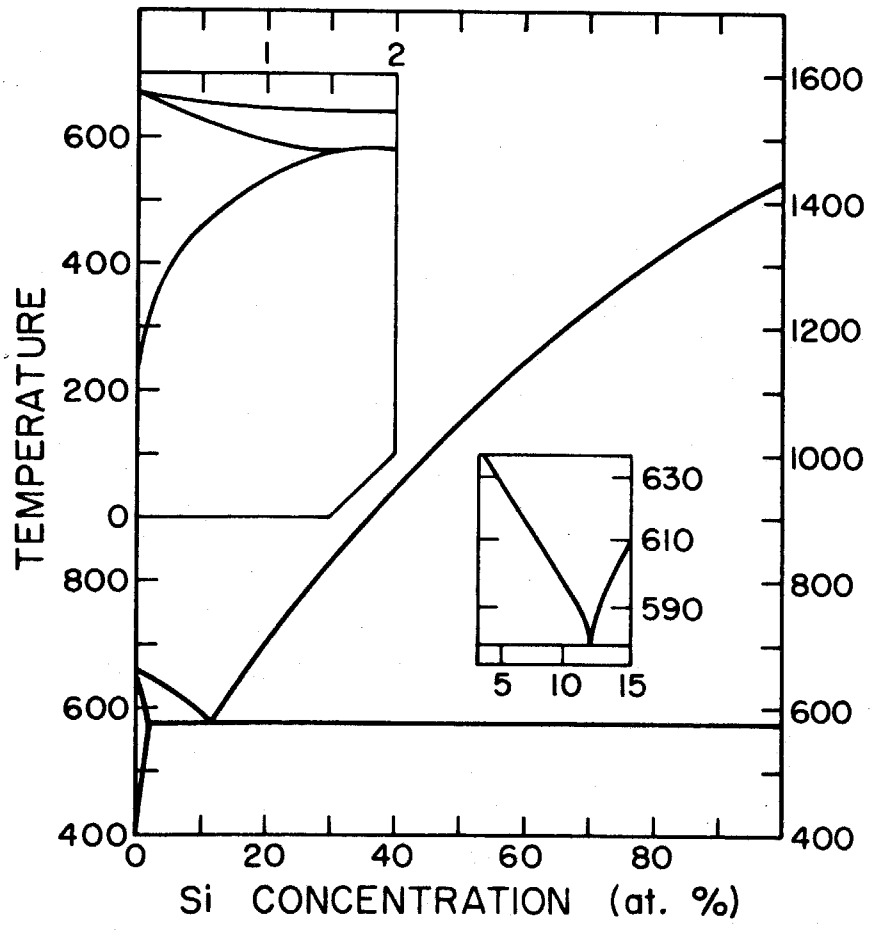

FIGURE 1. Phase Diagram of Al-Si (From Ref. 9)

the disappearance of the energy gap of the semiconductor for Pb-rich alloys. For this reason, the present study was confined to simple eutectic alloys.

The scale of the microstructure (i.e., the characteristic size of the interspersed metal and semiconducting domains) varies greatly among simple eutectic alloys. The effect of an interface interaction on the electronic properties of the metal domains depends on the surface-to-volume ratio of the metal domain. Thus, domain size is a critical parameter in the study of such interactions. This parameter can be varied for a given alloy system by varying the cooling rate of the alloy from the liquid state, the scale being reduced as the cooling rate is increased. It is desirable that the scale of microstructure tends to be small in equilibrium.

Finally, a few remarks should be made concerning the nature of the metal-semiconductor interfaces obtained in eutectic alloys. In general, the dissimilarity between the x-stal structure of the metals studied and that of Si or Ge (diamond cubic) results in an incoherent interface. It is likely that no regular epitaxial structure exists at the interface. Furthermore, it is not even clear how well the interface can be defined on the atomic scale. Since the structure of the interface determines the characteristics of electronic wave functions in this region, it is clear that this structure must be an essential feature in any description of an interface interaction. Unfortunately, very little is known about this aspect of the problem since it involves structural details on the scale of a few atomic distances. In this respect, the study of thin films has an advantage.

Low energy electron diffraction can be used to study surfaces of thin films directly. (Reference 8.) Under restricted conditions, thin-metal films can be deposited epitaxially on substrates consisting of a single crystal of semiconducting or insulating material and the interface can be well-characterized. (Reference 8.) Such a detailed characterization is not possible in the present case.

II. EXPERIMENTAL PROCEDURES

The alloys studied contain x at.% of a metal A and 100-x at.% of a semiconductor B. Their compositions are given in Table I. The alloys were prepared by induction melting of the appropriate quantities of constituents in glassy carbon, alumina, and quartz crucibles under an Argon atmosphere. It was found that Al and Be alloys made in quartz are contaminated by reaction with the crucible and thus these alloys were prepared in dense alumina crucibles only. The purity of the Ge and Si used was 99.999%, and that of the metals was 99.99%, except Be, which was 99%. The as-cast samples were drawn into 2 mm rods from the melt. The quenched alloys were prepared by rapid cooling from the liquid state following a technique described in Reference 10. The cooling rate is estimated to be on the order of 10^6 ^{o}C/sec. The samples obtained using this method are of the form of irregularly shaped foils having a typical area of $\sim$ 1 cm^2 and a thickness ranging from 1 to 10 μm.

To determine the crystal structure and microstructure of the alloys, techniques of scanning electron microscopy (SEM) and x-ray diffraction were used. The crystal structure of each sample used for measurements of electrical resistivity, magnetization, etc., was checked by x-ray scanning using a Norelco diffractometer (copper K_α radiation, nickle filtered). At least one sample of each as-cast and liquid-quenched alloy was subsequently powdered and used to obtain a Debye-Scherrer film. The lattice parameters of the phases present

Constituents		At.% of A In
A	B	$A_x B_{100-x}$
Al	Ge	5, 10, 25, 50, 70
Al	Si	10, 25, 50, 60, 70, 75 80, 85, 90, 95, 97.5, 99
Ga	Ge	10, 50
Ga	Si	10, 50
Sn	Ge	10, 20, 70
Pb	Ge	2, 5, 10, 20, 70
In	Ge	10, 70
Tl	Ge	10, 70
Be	Si	25, 45, 62, 90

TABLE I. Composition of the Alloys Studied

were then computed from the Debye-Scherrer films using the Nelson-Riley extrapolation function.

The liquid-quenched sample foils used for the SEM study were mounted in such a manner as to expose a cross-section of the foil thickness along the copper substrate on which the foil was obtained. The samples were appropriately etched so as to obtain enhanced contrast between the component phases. Energy dispersive analysis of the secondary x-ray emission spectrum was used in conjunction with SEM to identify phases observed in the microstructure.

Electrical resistivity as a function of temperature was measured using a standard four-probe technique for temperatures ranging down to $1.3^{o}K$. The temperature was measured with a germanium resistance thermometer with an accuracy of $\pm 0.05^{o}K$. Two techniques were used to attach voltage leads to the quenched foils. The leads were spot-welded to some samples, whereas a pressure contact consisting of a clamped silver foil was used for other samples.

The superconducting transitions were also observed with a standard ac bridge technique using a frequency of 1 kHz. The relative inductance of a coil containing the sample is plotted as a function of temperature on an x-y recorder. The estimated peak-to-peak magnetic field at the specimen location is on the order of a few Gauss. Magnetization as a function of magnetic field strength was measured using a standard Farady magnetometer. In order to obtain a sufficient quantity (about 50 mg) of the liquid-quenched alloys for the magnetization measurement, it was necessary to combine the powder obtained from several (6-10) foils of a given alloy. The magnetization measurements

thus represent an average of several samples. Magnetoresistivity was measured for both the parallel and transverse orientation of current with respect to magnetic field at temperatures ranging from $1.3^{o}K$ to $4.2^{o}K$ and fields in the range 0-10 kG. The temperature for the magnetoresistivity measurements was measured with a gallium-arsenide resistance thermometer with an accuracy of $\pm 0.05^{o}K$.

III. RESULTS

Alloys were studied in both the as-cast form and the liquid-quenched form. Most of the results here are for Al alloys, since the most extensive work was done on these.

A. As-cast Aluminum Alloys

1. Microstructure and X-stal Structure

The x-ray diffraction analysis indicates that all as-cast alloys consist of two phases as expected from the equilibrium phase diagrams. The lattice parameters of each phase were found to be nearly independent of the alloy composition. A summary of the results is given in Table II. For example, the alloy $Al_{70}Si_{30}$ gives a lattice parameter of 4.048 ± 0.002Å for Al and 5.432 ± 0.002Å for Si. This compares to lattice parameters of 4.049Å and 5.430Å (Reference 11) obtained for the pure elements. The comparison indicates that there is very limited mutual solid solubility of the two phases present. The equilibrium phase diagram for Al-Si (Figure 1) gives the solubility of Si in Al as less than 0.1 at.% at room temperature and a maximum of ∿ 1.6 at.% at 577°C. The solubility of Al in Si is given as negligible.

SEM studies reveal the microstructure of the as-cast alloys. The general features of the Al-Si and Al-Ge microstructure resemble those reported in previous metallographic studies. (References 12 and 13.) For as-cast Al-Ge samples, typical Al domains are lamellar in form and have a characteristic thickness ranging from about 500Å to

Alloy	Phases Present	Lattice Parameters (Å)	T_c' (°K)	T_c
$Al_{5-70}Ge_{95-30}$	Al (f.c.c.) Ge (d.c.)	4.056 - 4.052 ± 0.002 5.656 ± 0.002	2.7-2.0	1.7-1.85
$Al_{10-99}Si_{90-1}$	Al (f.c.c.) Si (d.c.)	4.048 ± 0.002 5.432 ± 0.002	2.0-1.9	<1.3-1.55
$Ga_{10,50}Ge_{90,50}$	Ga (?) Ge (d.c.)	Not Determined 5.657 ± 0.005	6.5, 3.0	3.0, <1.3
$Ga_{10}Si_{90}$	Ga (?) Si (d.c.)	Not Determined 5.430 ± 0.005	6.5	2.5
$Sn_{10-70}Ge_{90-30}$	Sn (tetragonal) Ge (d.c.)	a = 3.180 ± 0.005 c = 5.830 ± 0.005 5.658 ± 0.005	3.8-3.9	3.5-3.7
$Pb_{2-70}Ge_{98-30}$	Pb (f.c.c.) Ge (d.c.)	4.950 ± 0.005 5.656 ± 0.005	7.25	<1.3-7.2
$In_{10,70}Ge_{90,30}$	In (tetragonal) Ge (d.c.)	a = 3.250 ± 0.005 c = 4.945 ± 0.005 5.656 ± 0.005	3.4	3.0-3.3
$Tl_{10,70}Ge_{90,30}$	Tl (h.c.p.) Ge (d.c.)	Not Determined	2.4	2.0-2.3
$Be_{25-90}Si_{75-10}$	Be (h.c.p.) Si (d.c.)	a = 2.275 ± 0.005 c = 3.610 ± 0.005 a = 5.426 ± 0.005	<1.3	<1.3

TABLE II. Summary of X-ray Analysis Results and Superconducting Transition Temperatures (Determined From Electrical Resistivity) for As-cast Alloys.

3500Å. A scanning electron micrograph is shown in Figure 2(a). Formation of lamellar colonies is noticeable. The effect of annealing the as-cast $Al_{70}Ge_{30}$ alloy at 400°C for one day is illustrated in Figure 2(b). The characteristic domain size is increased to the order of 5,000Å to 10,000Å. The microstructure of as-cast $Al_{70}Si_{30}$ is shown in a metallograph in Figure 2(c). An irregular eutectic structure (composition $Al_{89}Si_{11}$) is observed and characterized by a network of fan-shaped Si crystals surrounded by Al. Large (~10 μm) primary Si crystals are also observed along with the eutectic structure.

2. Electrical Resistivity

Superconducting transitions in the as-cast alloys were observed as a function of temperature, magnetic field, composition, and heat treatment. Electrical resistivity as a function of temperature for as-cast $Al_{70}Ge_{30}$ and $Al_{70}Si_{30}$ is shown in Figure 4. The resistivity begins to drop at an onset temperature defined as T_c' and falls sharply to a value less than 10^{-9} Ωcm at a temperature defined as T_c. For $Al_{70}Ge_{30}$ $T_c' \cong 2^oK$ and $T_c = 1.85^oK$. For $Al_{70}Si_{30}$ $T_c' \cong 1.9^oK$ and $T_c = 1.5^oK$. Critical current density (J_c) measurements at 1.3°K in zero magnetic field give values on the order of 10^3 A/cm^2 for both alloys.

For these alloys, annealing at 500°C (and at 200°C or 400°C) for one to eight days produced no observable effect on T_c. The electrical resistivity of an annealed sample is shown in Figure 4. The transition is observed to sharpen somewhat, resulting in slightly lower values of T_c'. Critical current density measurements on samples

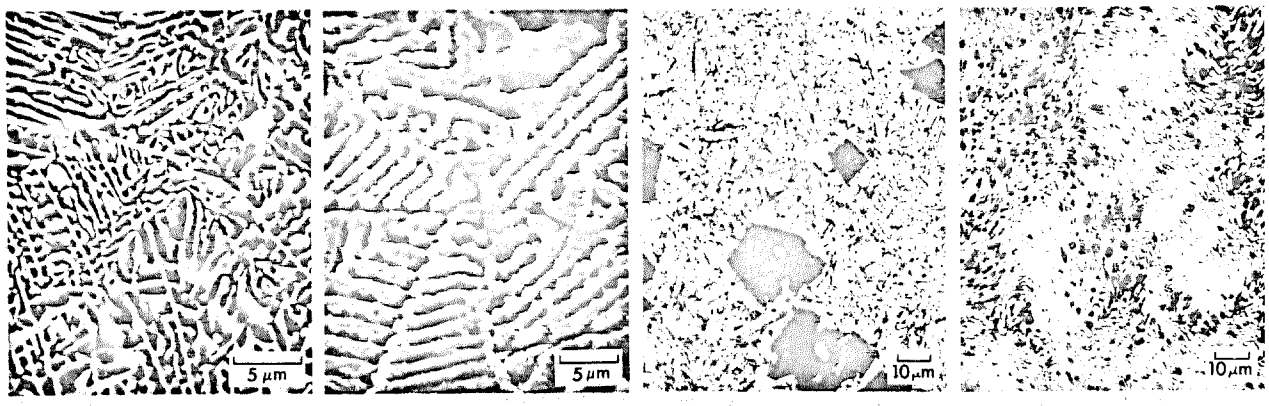

FIGURE 2. Scanning Electron Micrographs of (a) As-cast $Al_{70}Ge_{30}$, (b) As-cast $Al_{70}Ge_{30}$ Annealed at 400°C for 1 day; and Metallographs of (c) As-cast $Al_{70}Si_{30}$, and (d) As-cast $Al_{82}Cu_{18}$.

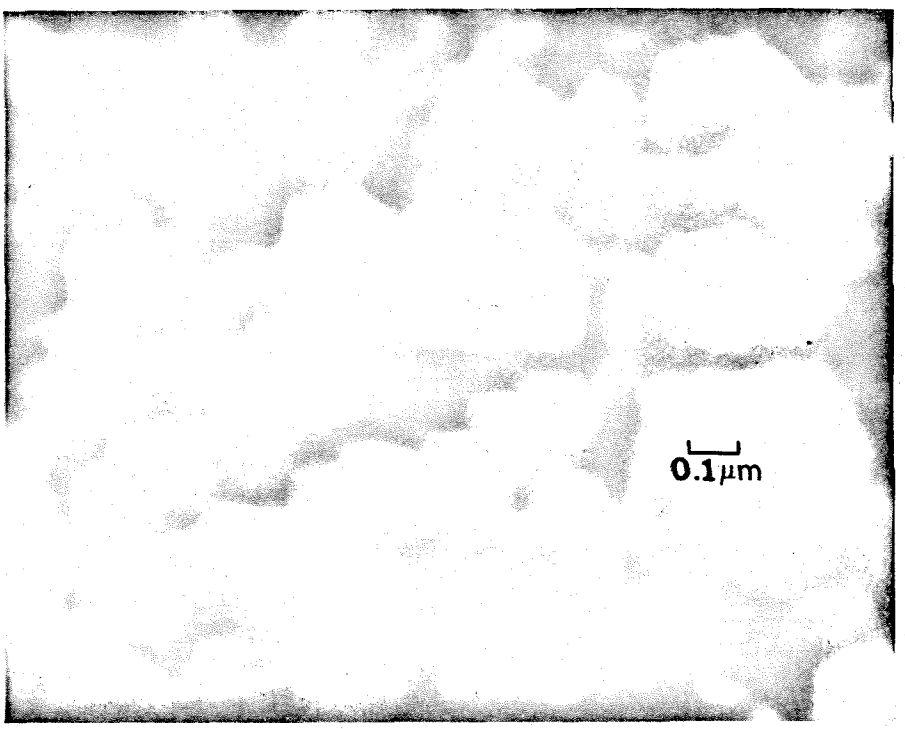

FIGURE 3. Scanning Electron Micrograph of Liquid-quenched $Al_{70}Si_{30}$ Showing a Region Near the Copper Substrate.

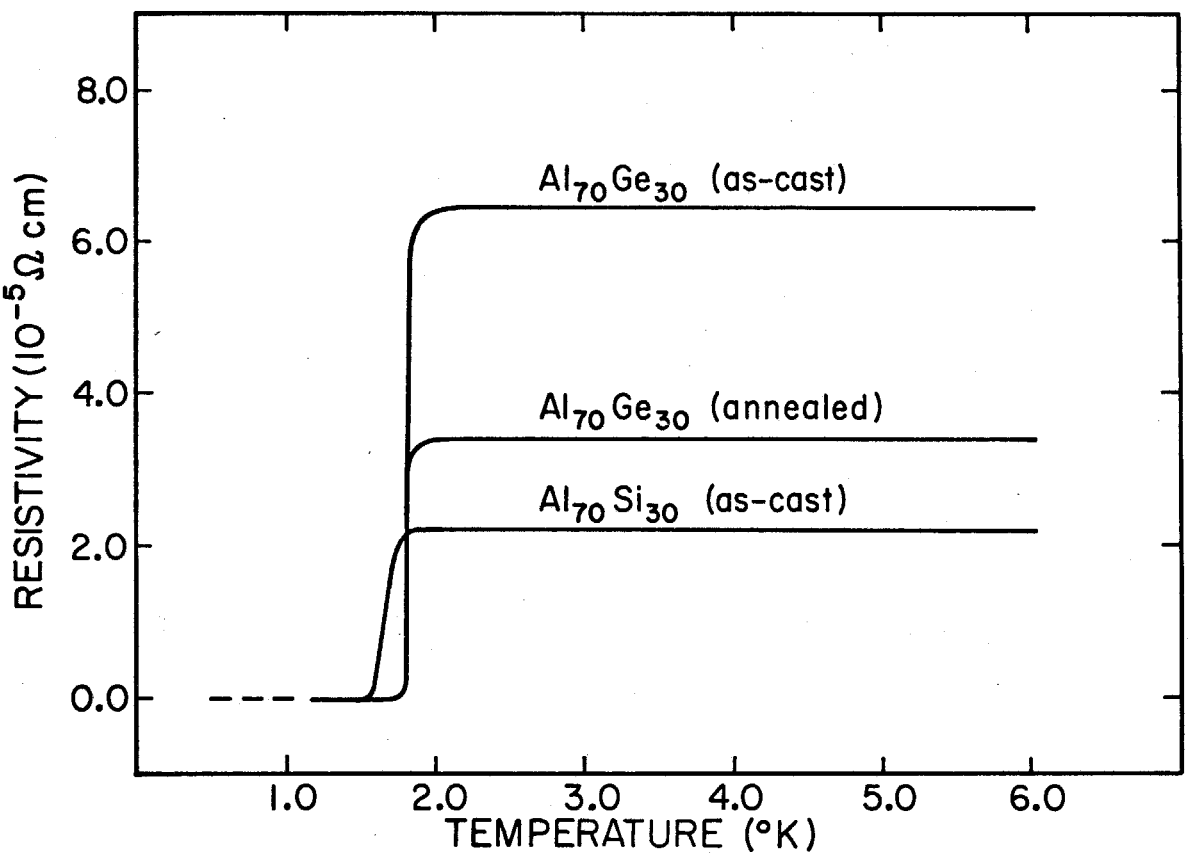

FIGURE 4. Electrical Resistivity As A Function Of Temperature For As-cast $Al_{70}Ge_{30}$, $Al_{70}Si_{30}$, And $Al_{70}Ge_{30}$ Annealed At 400°C For 1 Day.

annealed at 400°C indicate that J_c is reduced by about one order of magnitude compared to the J_c of as-cast samples.

The effect of a magnetic field on the resistive transition of the as-cast alloys at 1.3°K is shown in Figures 5 and 6. For $Al_{70}Ge_{30}$, a sharp resistive transition occurs at a field of 85G, and for $Al_{70}Si_{30}$ a similar transition occurs at 40G; however, a small amount of superconductivity persists to much higher fields (approximately 3kG for $Al_{70}Ge_{30}$). The resistive transition was observed to be independent of field orientation with respect to current direction. The critical current density (J_c) as a function of magnetic field at T = 1.3°K is shown in Figure 7.

The composition of the Al-Si and Al-Ge alloys was varied as indicated in Table I. The transition temperature, as measured by resistivity, was found to be nearly independent of composition. For low Al concentrations (e.g., Al_5Ge_{95}) T_c remains unchanged, while T_c' is found to be slightly higher ($\sim$2.7°K), as shown in Figure 8. The critical current density is of order 10 A/cm^2 for Al_5Ge_{95}. A resistive transition for $Al_{50}Si_{50}$ is shown in Figure 8. A summary of electrical resistivity measurements on as-cast Al-Ge and Al-Si alloys is given in Table III.

3. Magnetic Measurements

Relative inductance change as a function of temperature using a standard ac bridge for $Al_{70}Ge_{30}$ and $Al_{70}Si_{30}$ is shown in Figure 9. A large inductive transition occurs at a slightly lower temperature ($\sim$0.1°K) than that of the resistive transition shown in Figure 4.

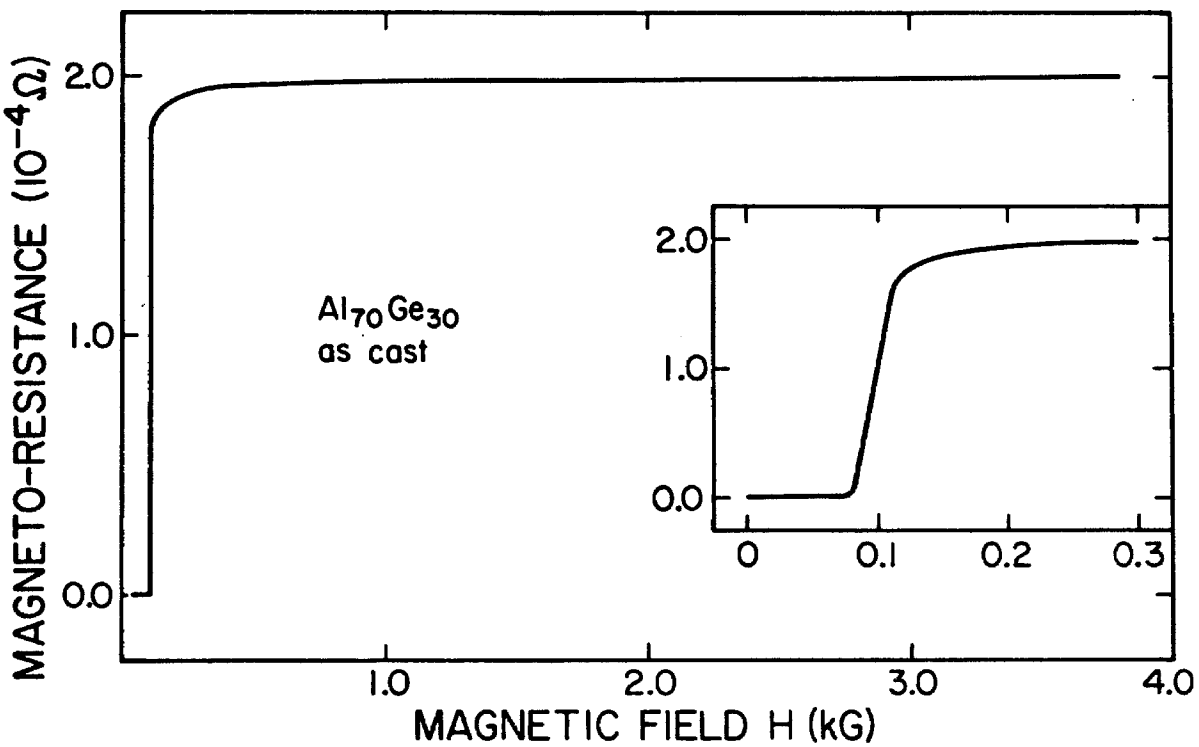

FIGURE 5. Longitudinal Magneto Resistance at 1.3°K for $Al_{70}Ge_{30}$ As-cast. The Insert Shows the Low Field Behavior.

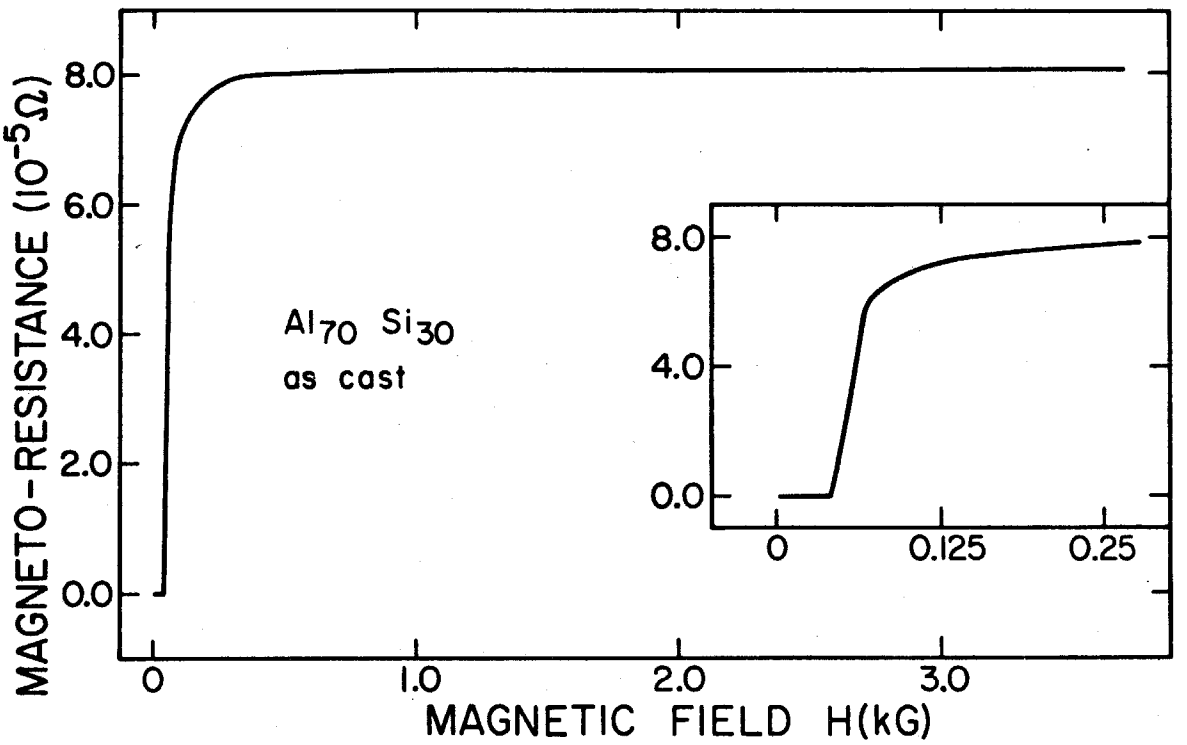

FIGURE 6. Longitudinal Magneto Resistance at 1.3°K for $Al_{70}Si_{30}$ As-cast. The Insert Shows the Low Field Behavior.

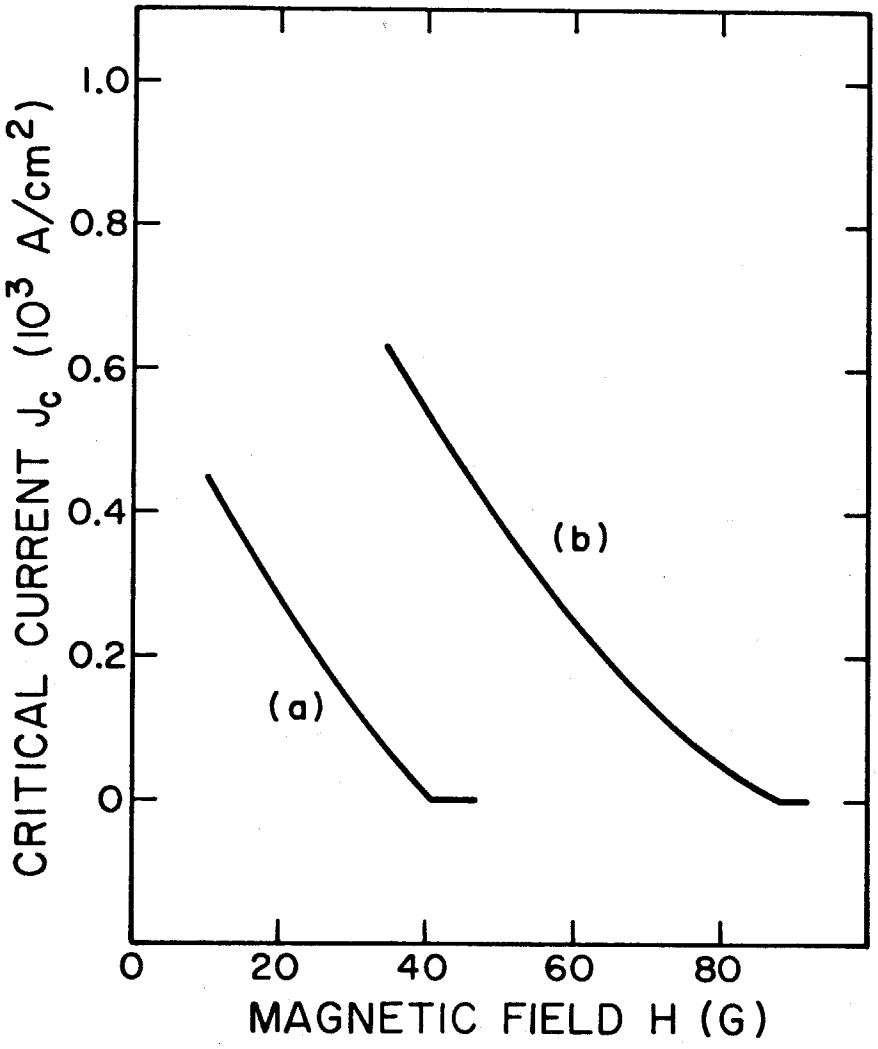

FIGURE 7. Critical Current J_c at 1.3°K as a Function of Magnetic Field for (a) As-cast $Al_{70}Si_{30}$ and (b) As-cast $Al_{70}Ge_{30}$.

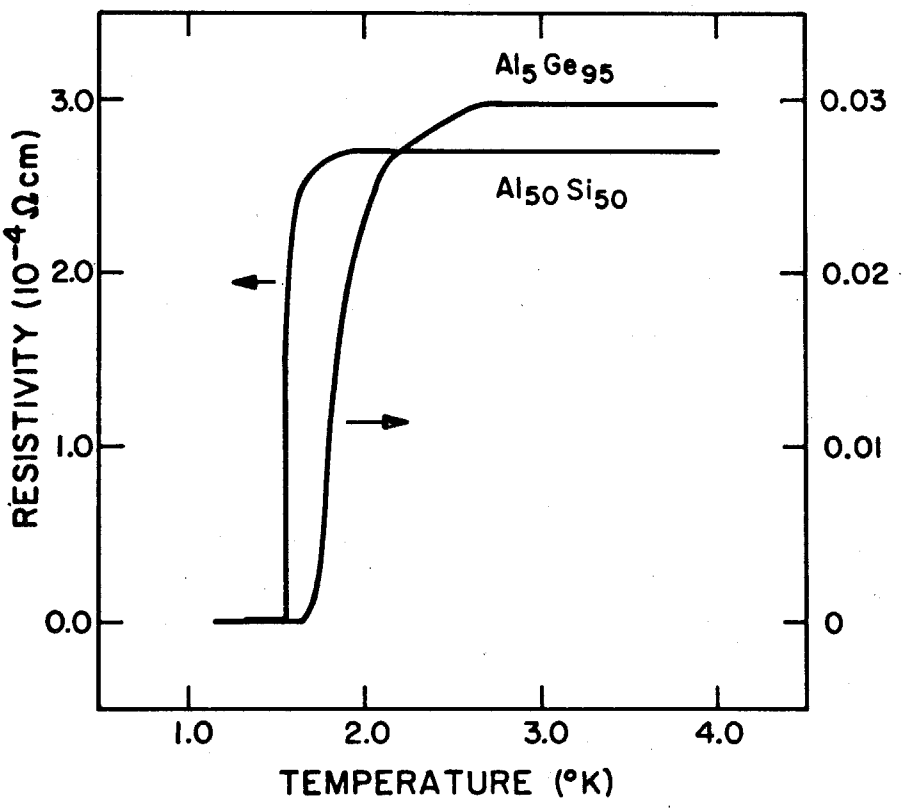

FIGURE 8. Electrical Resistivity as a Function of Temperature for Al_5Ge_{95} (Right Hand Scale in Ωcm) and $Al_{50}Si_{50}$ (Left Hand Scale in 10^{-4} Ωcm) As-cast.

Alloy	Phases Present	Lattice Parameters (Å)	T_c' (°K)	T_c (°K)	Estimated Residual Resistivity (10^{-6} Ωcm)
$Al_{99}Si_1$	Al (f.c.c.)	4.047 ± 0.002	<1.3	<1.3	5
$Al_{97.5}Si_{2.5}$	Al (f.c.c.)	4.045 ± 0.002	1.5	1.3	10
$Al_{95}Si_5$	Al (f.c.c.)	4.044 ± 0.002	2.4	1.7	15
$Al_{90}Si_{10}$	Al (f.c.c.) Si (d.c.)	4.042 ± 0.002 5.432 ± 0.003	3.9	2.2	25
$Al_{85}Si_{15}$	Al (f.c.c.) n Si (d.c.)	4.040 ± 0.002 5.433 ± 0.003	5.1	3.3	60
$Al_{80}Si_{20}$	Al (f.c.c.) Si (d.c.)	4.042 ± 0.002 5.433 ± 0.003	6.0	4.0	90
$Al_{75}Si_{25}$	Al (f.c.c.) Si (d.c.)	4.043 ± 0.002 5.432 ± 0.002	6.2	5.6	120
$Al_{70}Si_{30}$	Al (f.c.c.) Si (d.c.)	4.044 ± 0.002 5.434 ± 0.003	6.5	5.5	150
$Al_{60}Si_{40}$	Al (f.c.c.) Si (d.c.)	4.044 ± 0.002 5.434 ± 0.003	7.5	4.0	200
$Al_{50-10}Si_{50-90}$	Al (f.c.c.) Si (d.c.)	4.044 - 4.047 ~5.432 (constant)	<7.5	<4.0	>300

TABLE III. Summary of Results of X-ray Analysis and Superconducting Transition Temperature (From Electrical Resistivity) for Liquid-Quenched Alloys.

Alloy	Phases Present	Lattice Parameters (Å)	T_c' (°K)	T_c (°K)	Estimated Residual Resistivity (10^{-6} Ωcm)
$Al_{70}Ge_{30}$	Al_2Ge (tetragonal) Other Phase	See Refs. 16 and 17	6.0	3.0	100
	Al (f.c.c.)	4.052 ± 0.003			
	Ge (d.c.)	5.664 ± 0.005			
$Al_{50}Ge_{50}$	Same As $Al_{70}Ge_{30}$	4.052 ± 0.003 5.662 ± 0.005	6.0	2.0	300
$Ga_{10}Ge_{90}$	Ga (?) Ge (d.c.)	Not Determined	8.0	3.2	
$Ga_{50}Ge_{50}$	Ga (?) Ge (d.c.)	Not Determined	2.5	1.7	
$Sn_{20}Ge_{80}$	Sn (tetragonal) Ge (d.c.)		4.5	3.7	
$Sn_{70}Ge_{30}$	Sn (tetragonal) Ge (d.c.)	a = 3.184 ± 0.003 c = 5.827 ± 0.005 5.665 ± 0.005	6.5	3.8	
$Pb_{20}Ge_{80}$	Pb (f.c.c.) Ge (d.c.)		7.4	6.5	
$Pb_{70}Ge_{30}$	Pb (f.c.c.) Ge (d.c.)	4.949 ± 0.002 5.659 ± 0.005	7.8	6.9	

TABLE III (Continued)

Alloy	Phases Present	Lattice Parameters (Å)	T_c' (°K)	T_c (°K)	Estimated Residual Resistivity (10^{-6} Ωcm)
$In_{10,70}Ge_{90,30}$	In (tetragonal) Ge (d.c.)		3.4	<3.4	
$Tl_{10,70}Ge_{90,30}$	Tl (h.c.p.) Ge (d.c.)		2.4	<2.4	
$Be_{25}Si_{75}$	Be (h.c.p.) Si (d.c.)		~4.0	~1.2	
$Be_{45}Si_{55}$	Be (h.c.p.) Si (d.c.)	a = 2.265 ± 0.005 c = 3.610 ± 0.005 5.426 ± 0.005	~9.0	~1.2	
$Be_{62}Si_{38}$	Be (h.c.p.) Si (d.c.)	a = 2.268 ± 0.005 c = 3.612 ± 0.005 5.426 ± 0.005	~9.0	<1.2	
$Be_{90}Si_{10}$	Be (h.c.p.) Si (d.c.)	a = 2.270 ± 0.01 c = 3.610 ± 0.01 5.425 ± 0.005	<1.2	<1.2	

TABLE III (Continued)

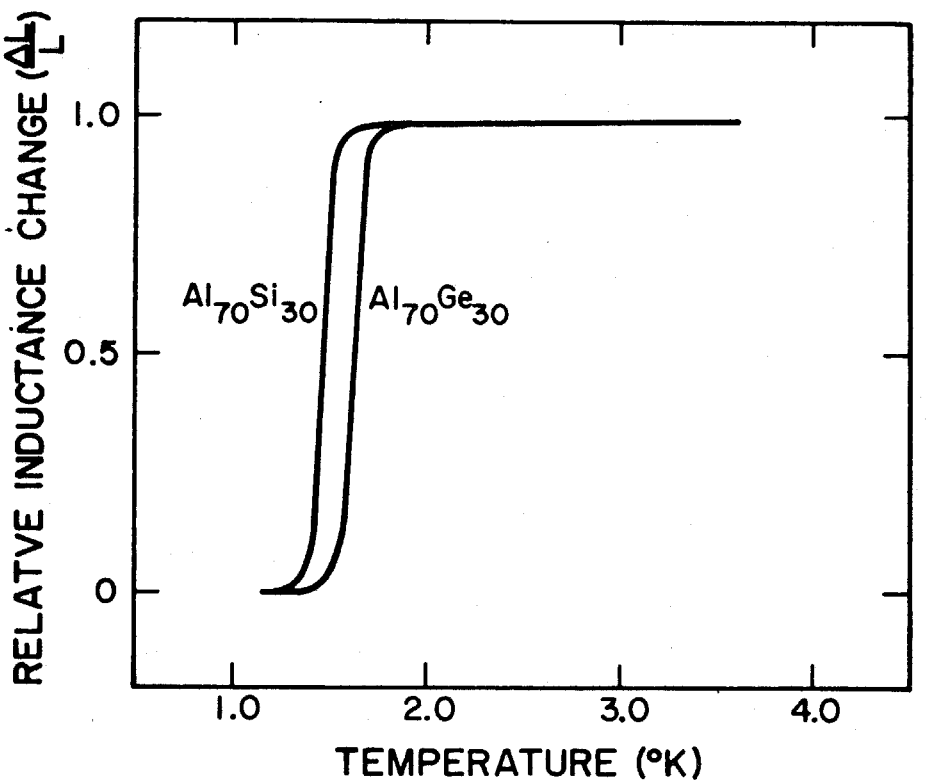

FIGURE 9. Relative Inductance Change as a Function of Temperature for As-cast $Al_{70}Ge_{30}$ and $Al_{70}Si_{30}$.

Typical results of dc magnetization measurements at 1.3°K for $Al_{70}Ge_{30}$ are shown in Figure 10. As a function of field, a constant diamagnetic susceptibility up to a field of 25G is observed. With increasing fields above 25G, type II magnetic behavior is observed. A small amount of superconductivity persists in fields up to approximately 7kG. Magnetization as a function of field for $Al_{70}Si_{30}$ is similar to that of $Al_{70}Ge_{30}$.

B. Liquid-Quenched Aluminum Alloys

1. Crystal Structure and Microstructure

For liquid-quenched Al-Si alloys, x-ray diffraction studies indicate that no intermediate phases exist in agreement with previous work. (Reference 14.) A lattice parameter of 5.434 ± .003Å was found for the Si phase and was independent of Si concentration in the alloy. This indicates that no significant amount of Al is dissolved by the Si phase after liquid-quenching. On the other hand, the lattice parameter of the Al phase was found to vary slightly with increasing Si concentration in the alloy. A plot is shown in Figure 11. A Si phase is observed in Debye-Scherrer films for alloys containing more than 5 at.% of Si. This is apparently the limit for complete solubility of Si in the Al phase of the alloys. A slope change in the plot of the Al lattice parameter (Figure 11) occurs with increasing Si concentration at about 3 at.% Si. The slope change may be associated with the formation of Si precipitate. This behavior is in general agreement with previous studies. (Reference 15.) Table III contains a summary of x-ray results for liquid-quenched Al-Si alloys.

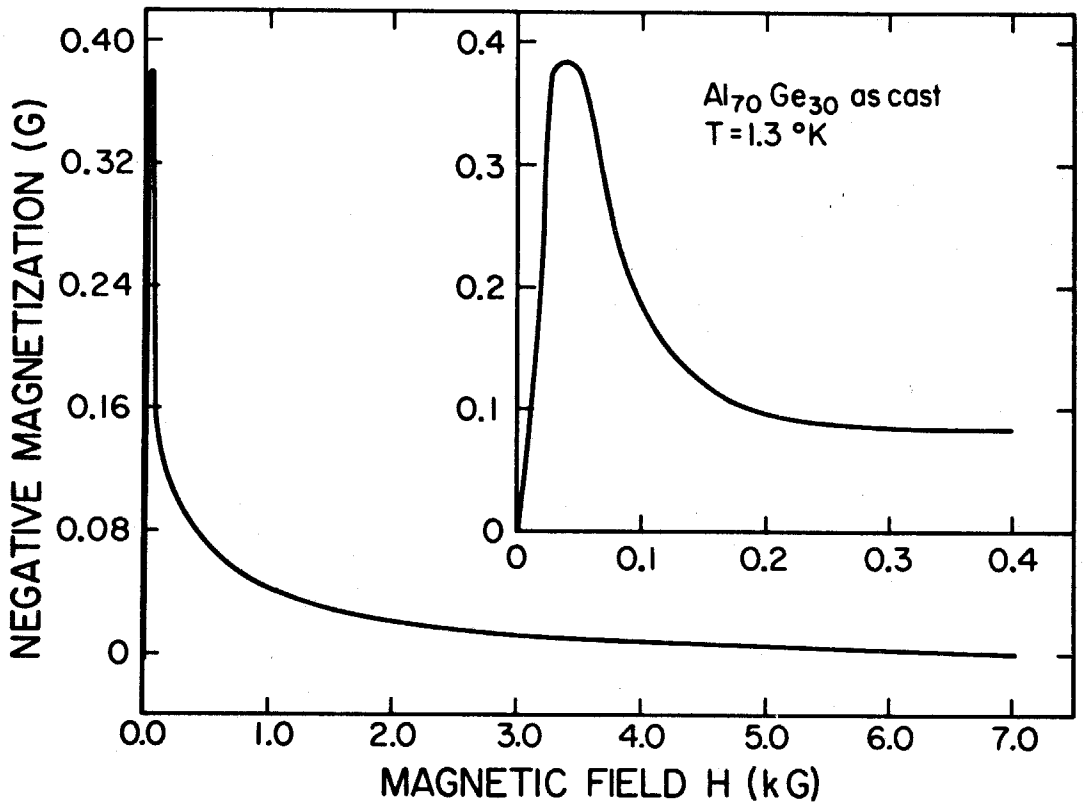

FIGURE 10. Magnetization as a Function of Magnetic Field for As-cast $Al_{70}Ge_{30}$.

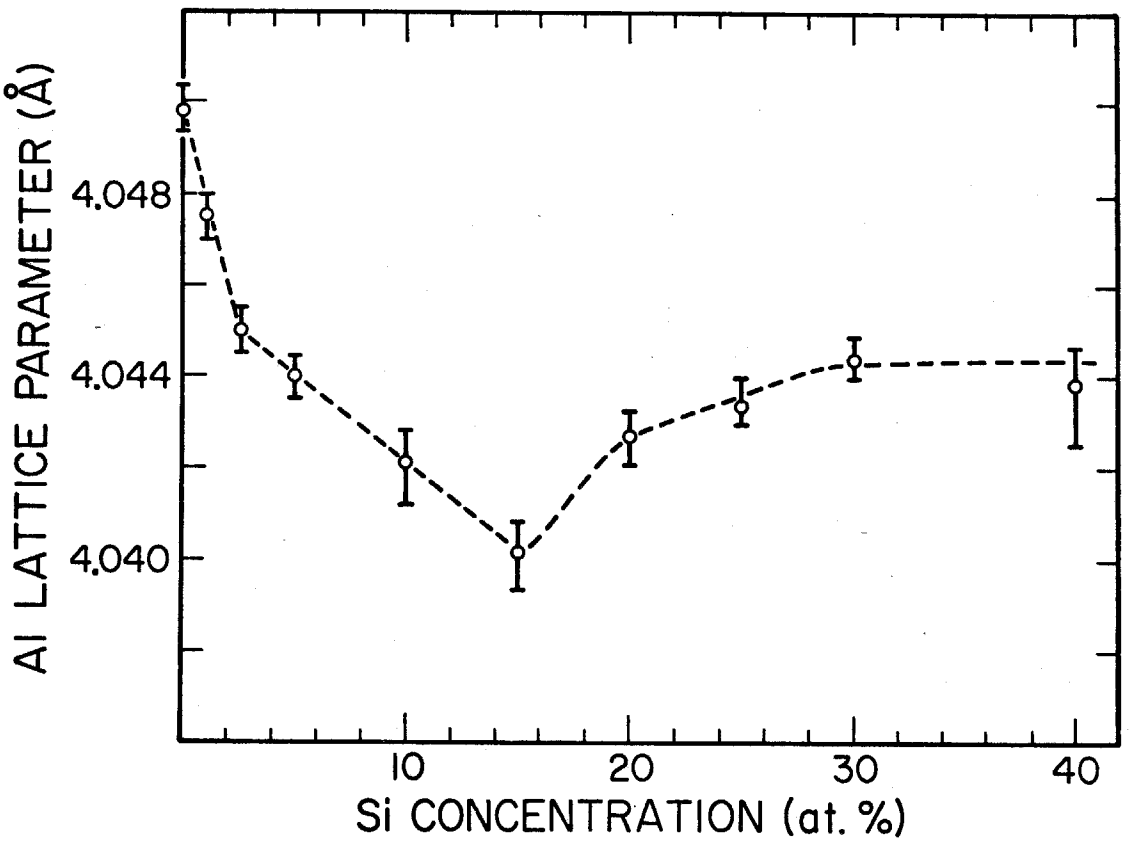

FIGURE 11. Lattice Parameter of the Al Phase in Liquid-Quenched Al-Si Alloys as a Function of Si Content.

Since it has been previously established that the microstructure of the Al-Si eutectic is extremely sensitive to the cooling rate from the melt (Reference 13), it is expected that rapid-quenching from the liquid state can drastically alter it. The SEM studies on rapidly quenched Al-Si alloys substantiate this expectation. In the quenched samples, there is a spatial distribution of cooling rates. In the regions where the cooling rate is greatest (near the substrate), the eutectic composition is seen to be shifted to higher Si concentration. Si precipitate tends to cluster uniformly along the substrate. In Figure 3, a scanning electron micrograph of such a region near the copper substrate is shown for an $Al_{70}Si_{30}$ sample. In this region, Al domains ranging in size from $\sim$ 100Å to $\sim$ 1000Å can be seen interpenetrating a network of Si crystals, typically 500Å to 3000Å in size. For the alloy $Al_{85}Si_{15}$, similar precipitation of Si near the substrate was observed in scanning electron micrographs, although the amount of Si precipitate is reduced. The characteristic size of the Al domains in the region near the substrate remains about the same as that in $Al_{70}Si_{30}$. It should be noted that the type of microstructure observed in Figure 3 is quite uniformly and continuously distributed along the substrate.

X-ray analysis of liquid-quenched Al-Ge alloys confirm the previously reported presence of a metastable tetragonal Al_2Ge phase and another complex metastable phase, the crystal structure of which has not been determined. (References 16 and 17.) These intermediate metastable phases are found to decompose into Al and Ge following annealing at a temperature of 200°C for a period of one hour. Due to

the presence of these metastable phases, the liquid-quenched Al-Ge alloys were not studied in as much detail as the liquid-quenched Al-Si alloys.

2. Electrical Resistivity

Electrical resistance as a function of temperature for several liquid-quenched Al-Si alloys is shown in Figure 12. Due to the non-uniform thickness and irregular shape of the samples, it is difficult to accurately estimate the residual resistivity ρ_0. Approximate values of ρ_0 were obtained by estimating the average sample thickness to be 2-5 μm. This estimate is based on the measured weight of the samples and the estimated sample area. An independent check of the average sample thickness was also made using SEM micrographs. The estimated residual resistivities of Al-Si samples are included in Table III, along with a summary of x-ray results and superconducting transition temperatures T_c' and T_c. To illustrate the dependence of transition temperature on alloy composition, a plot of the transition temperature as a function of Si content of the alloy is shown in Figure 13. To best compare the alloys, the transition temperature is taken to be the temperature at which the sample resistance has dropped to half the residual value (henceforth referred to as $T_c^{\frac{1}{2}}$). It should be noted that the results of at least two samples have been averaged to determine each point in Figure 13. This procedure eliminates variations in $T_c^{\frac{1}{2}}$ due to uncontrollable differences in quenching rate (these variations were found to be small, $<0.2^{o}K$) of samples with the same composition. The superconducting transition temperature is

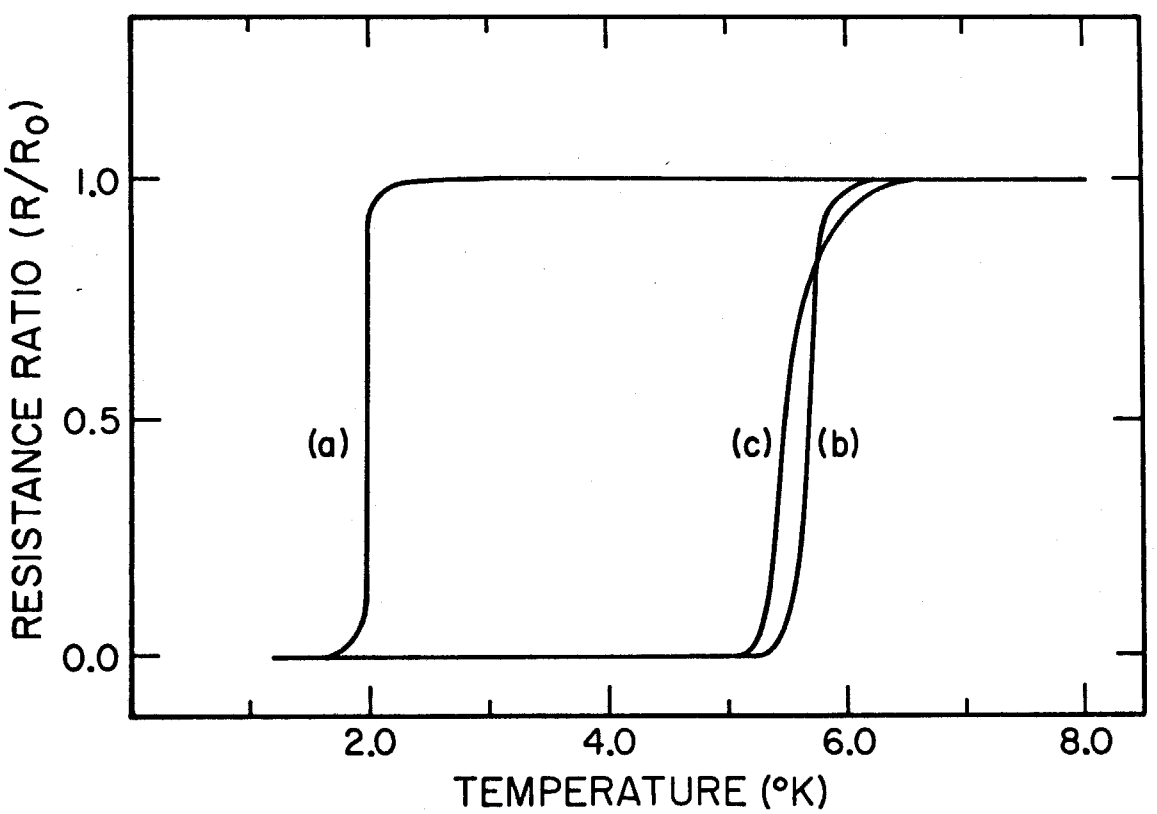

FIGURE 12. Electrical Resistance Ratio (R/R_0) (R_0 is the Residual Resistance at 8^oK) as a Function of Temperature for (a) $Al_{95}Si_5$, (b) $Al_{70}Si_{30}$, (c) $Al_{60}Si_{40}$ All Quenched From the Liquid State.

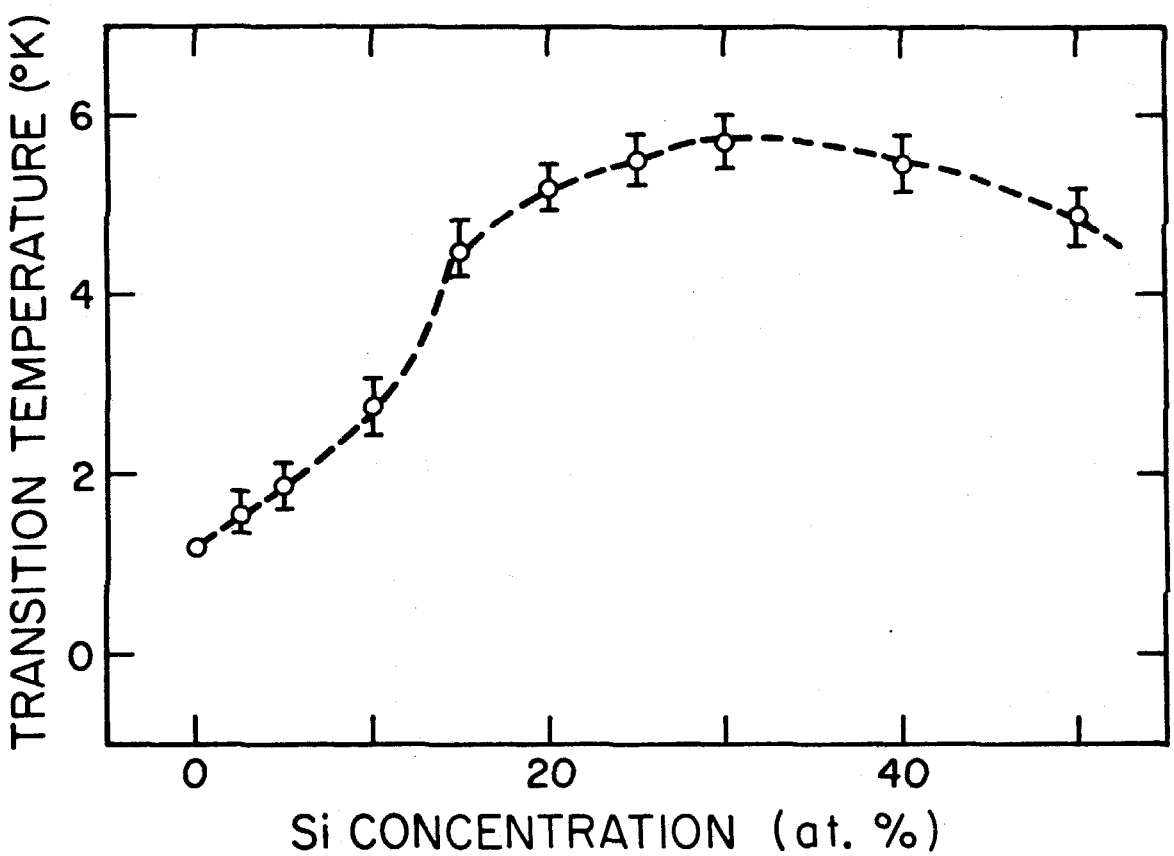

FIGURE 13. Superconducting Transition Temperature as a Function of Composition for Liquid-Quenched Al-Si Alloys.

seen to initially increase with increasing Si content of the alloy reaching a maximum at the composition $Al_{70}Si_{30}$ after which it decreases slowly. The onset temperature of the transition T_c' reaches 7.5^oK in some samples containing 40-50 at.% Si. A significant broadening of the transition accompanies additions of Si in excess of 30 at.%. For example, samples containing 50 at.% Si have transition widths ($T_c' - T_c$) as large as 3^oK. Similar results were found for Al-Ge alloys. The onset temperature T_c' reaches a maximum of $\sim 6.0^oK$ for the alloy $Al_{70}Ge_{30}$, while $T_c = 4.5^oK$; however, the new metastable crystalline phases make interpretation difficult.

The magnetoresistance of liquid-quenched $Al_{70}Si_{30}$ was measured for both the transverse and longitudinal orientations of field with respect to current and found to be independent of field orientation. A typical graph is shown in Figure 14. A broad magnetoresistive transition beginning at 3.5 Kg and ending at about 10 Kg is observed.

3. Magnetic Measurements

Results of the ac inductance bridge measurements for two quenched $Al_{70}Si_{30}$ samples are shown in Figure 15. The most striking feature of this result is the fact that complete expulsion of magnetic flux occurs only below about 1.3^oK. The result indicates that a rather small fraction of the sample shows a Meissner effect at temperatures above 5.0^oK, whereas the resistive transition of these samples is complete at this temperature. Magnetization as a function of applied field at 1.4^oK for liquid-quenched $Al_{70}Si_{30}$ is shown in Figure 16. The phenomenon of irreversible magnetization is observed.

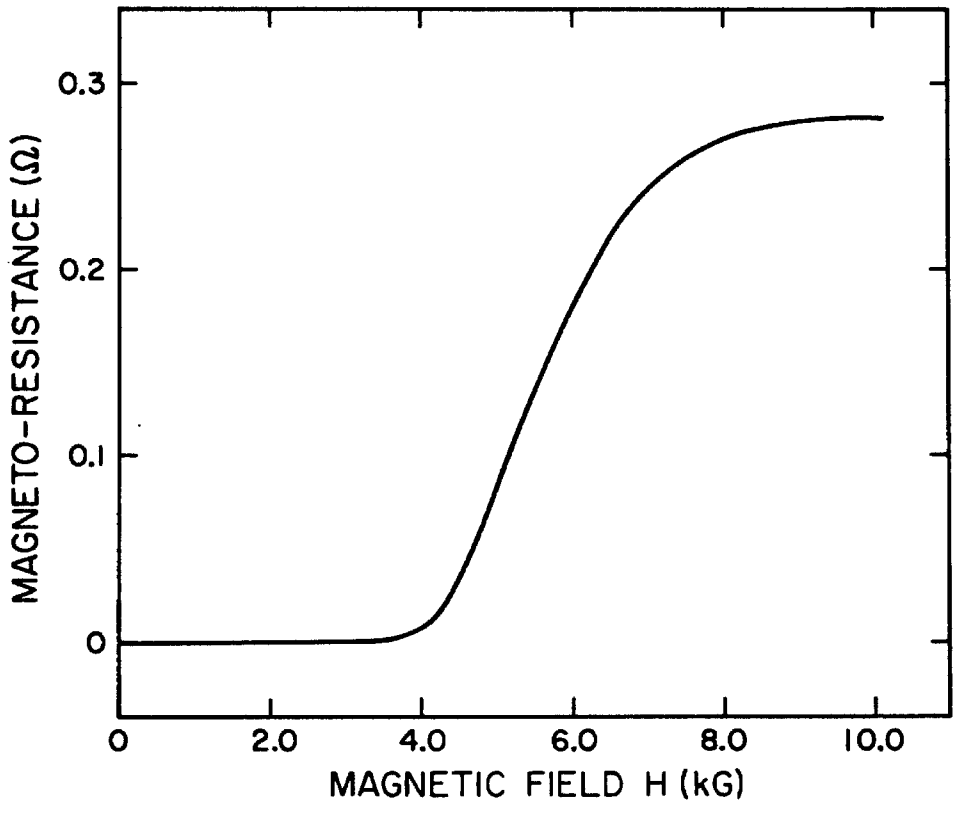

FIGURE 14. Longitudinal Magnetoresistance at $1.3^{o}K$ as a Function of Magnetic Field for Liquid-Quenched $Al_{70}Si_{30}$.

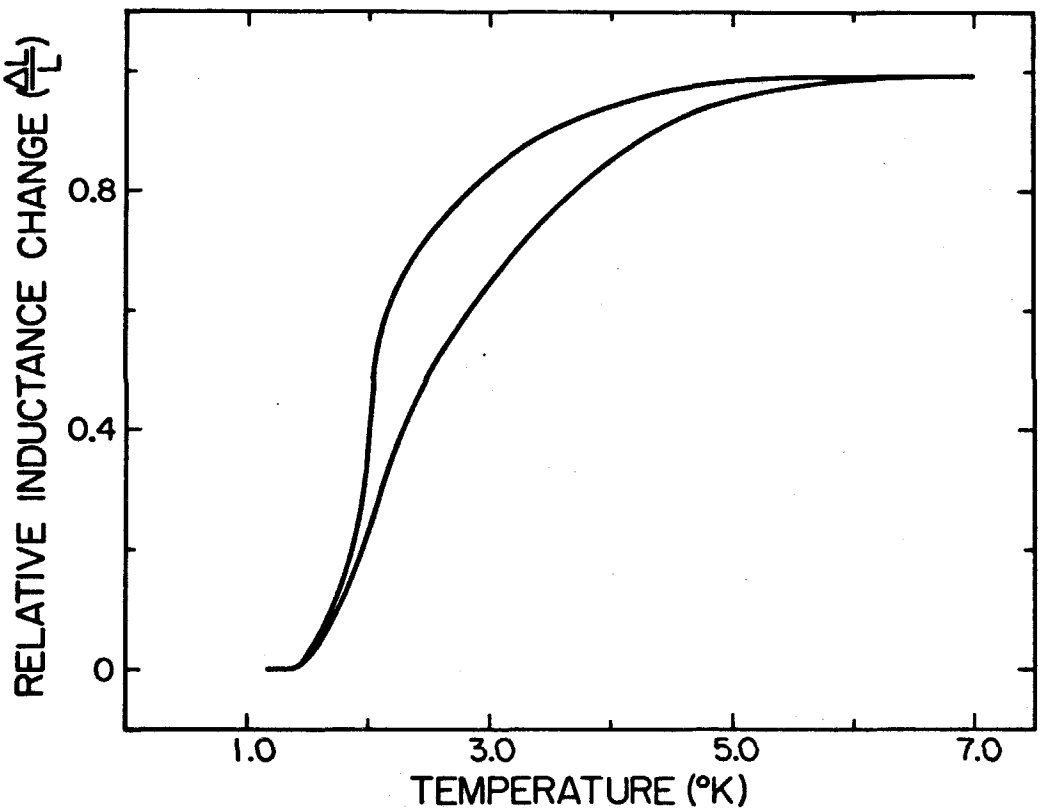

FIGURE 15. Relative Inductance Change as a Function of Temperature for Two Samples of Liquid-Quenched $Al_{70}Si_{30}$.

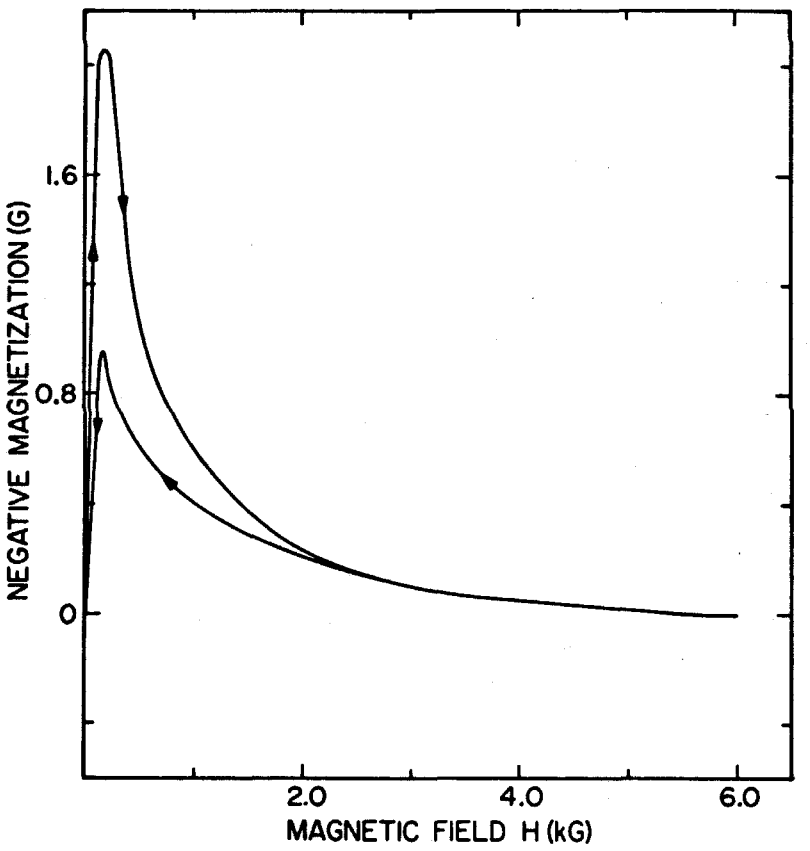

FIGURE 16. Magnetization as a Function of Magnetic Field at T = 1.4°K for $Al_{70}Si_{30}$ Quenched From the Liquid State. Arrows Indicate Direction of Field Change.

The sample shows linearly increasing negative magnetization (type I) behavior up to 100G. The absolute magnetization decreases sharply for fields exceeding 200G. Superconductivity persists in fields up to between 6 and 7 Kg. The overall behavior is that of a type II superconductor.

4. Annealing Behavior

The effect of annealing the liquid-quenched Al-Si alloys on the superconducting transition temperature was studied. For $Al_{70}Si_{30}$ samples, annealing at 100°C for periods of 1-4 hours results in a decrease of T_c to $\sim 3^oK$ and T_c' to $\sim 4^oK$ as measured by electrical resistivity. Annealing for longer periods at 100°C results in little additional change in T_c. The lattice parameter of the Al phase is observed to increase from 4.039 ± .002Å to 4.044 ± .002Å after this annealing. Annealing for 1-4 hours at 300°C results in a decrease of T_c to $\sim 2^oK$. Finally, annealing at 500°C for 1-4 hours results in a value of $T_c \cong 1.6^oK$ near that observed in as-cast $Al_{70}Si_{30}$ alloys. The lattice parameter of the Al phase in $Al_{70}Si_{30}$ alloys annealed at 300°C and 500°C is within experimental error (±.002Å) equal to that obtained in as-cast $Al_{70}Si_{30}$ alloys.

C. Results for Other Alloys

Of the other alloys investigated, only Ga-Ge and Ga-Si alloys showed an enhancement of the superconducting transition temperature of the metallic component in the as-cast condition. Other as-cast alloys were observed to have both T_c' and T_c less than or equal to T_{c0}, the transition temperature of the pure metal. The results for the

other as-cast alloys are summarized in Table II.

Table IV contains a summary of results for other liquid-quenched alloys. Included in the table are the composition of the alloys, the phases present in the alloys, lattice parameters obtained for the phases, the maximum observed onset temperature T_c', and the superconducting transition temperature T_c. To define T_c' and T_c, results of electrical resistivity measurements were used.

The liquid-quenched Sn-Ge alloys were studied by x-ray diffraction and found to contain only Sn and Ge. The superconducting transitions for these alloys are rather broad. For example, $T_c' = 6.5^oK$ and $T_c = 3.8^oK$ for the alloy $Sn_{70}Ge_{30}$, while $T_c' = 4.5^oK$ and $T_c = 3.6^oK$ for the alloy $Sn_{20}Ge_{80}$. Results of electrical resistivity measurements are shown in Figure 17. To demonstrate the effect of liquid-quenching on pure Sn, a measurement of relative inductance is shown, together with that of the liquid-quenched alloy $Sn_{20}Ge_{80}$ in Figure 18. The enhancement effect associated with the presence of Ge can be seen.

Relative inductance as a function of temperature for liquid-quenched $Ga_{10}Ge_{90}$ is shown in Figure 19, along with that of the same alloy in the as-cast condition. The presence of β Ga ($T_c = 6.4^oK$) (Reference 18) in the as-cast alloy is apparent; however, a much larger transition occurring just below 4^oK is also observed in this alloy. The electrical resistance of liquid-quenched $Ga_{10}Ge_{90}$ is shown in Figure 20, along with the electrical resistance of liquid-quenched $Ga_{50}Ge_{50}$. The transition temperature of alloys containing more than 10 at.% of Ga was observed to be less than that of $Ga_{10}Ge_{90}$. The onset temperature of T_c' of the latter alloy is seen to reach nearly 8^oK.

Metal	T_c (^oK) (Calorimetric)	T_c (^oK) (Magnetic)
Al	1.183	1.196
Ga (α)	1.087	1.091
(β)		6.2
(γ)		7.62
Sn	3.722	3.7222
Pb	7.23	7.193
In	3.407	3.4035
Tl	2.38	2.39
Be	<0.1	<0.1

TABLE IV. Superconducting Transition Temperatures of Pure Metals.*

*Data taken from the 1970 edition of the Handbook of Chemistry and Physics (The Chemical Rubber Co., Cleveland, Ohio, 1970).

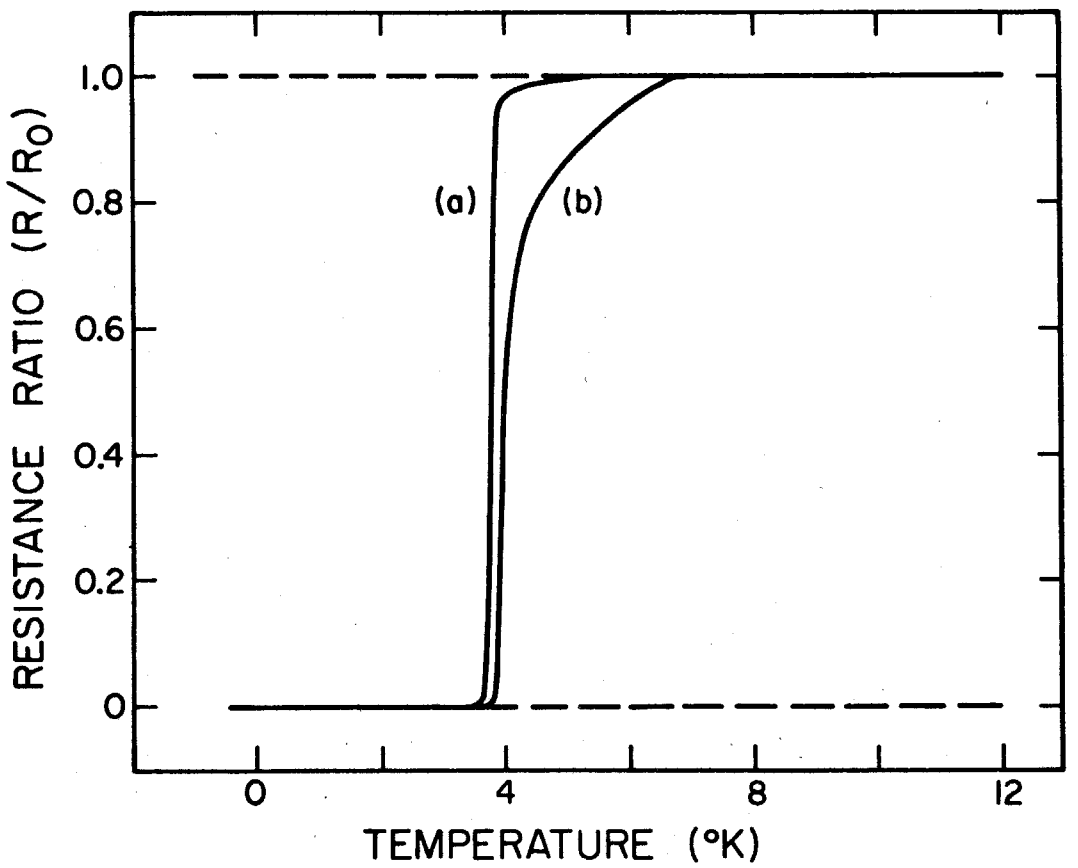

FIGURE 17. Electrical Resistance Ratio (R/R_0) (R_0 = Resistance at $10^{o}K$) as a Function of Temperature for (a) Liquid-Quenched $Sn_{20}Ge_{80}$, and (b) Liquid-Quenched $Sn_{70}Ge_{30}$.

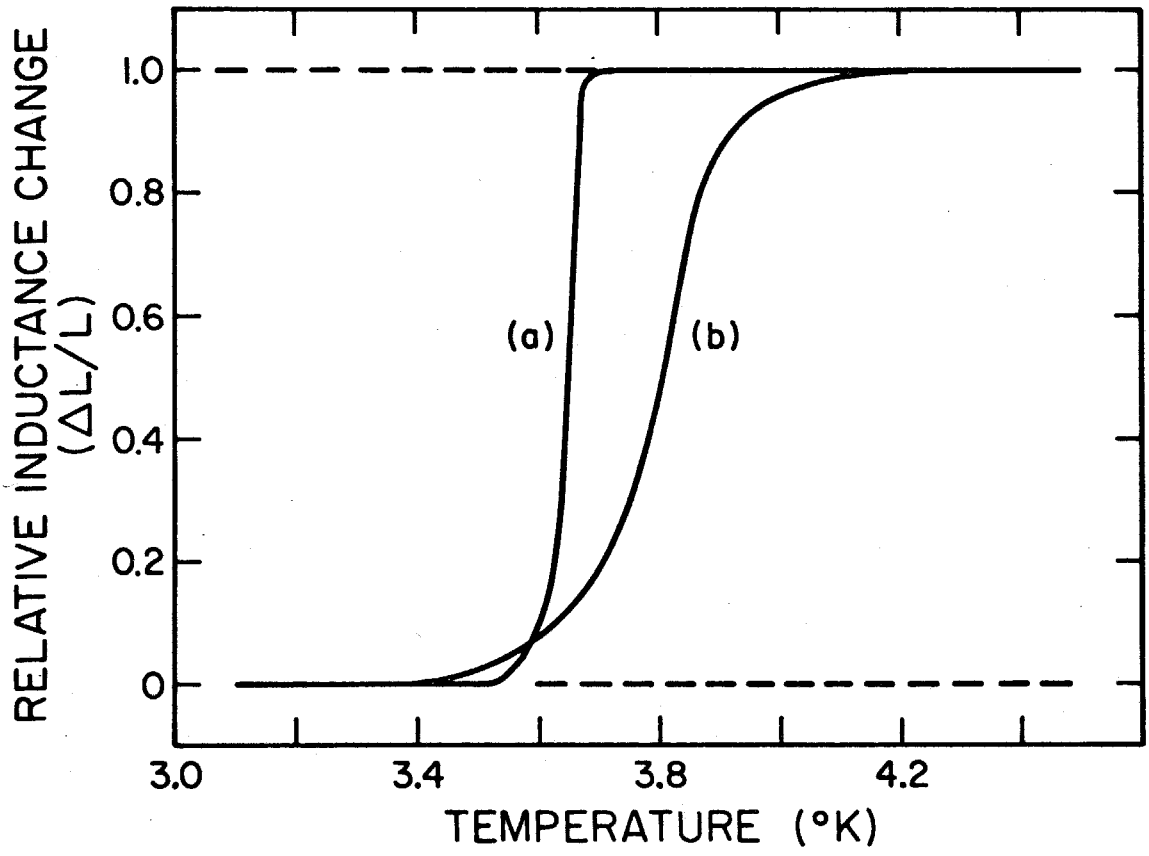

FIGURE 18. Relative Inductance Change as a Function of Temperature for (a) Liquid-Quenched Sn, and (b) Liquid-Quenched $Sn_{20}Ge_{80}$.

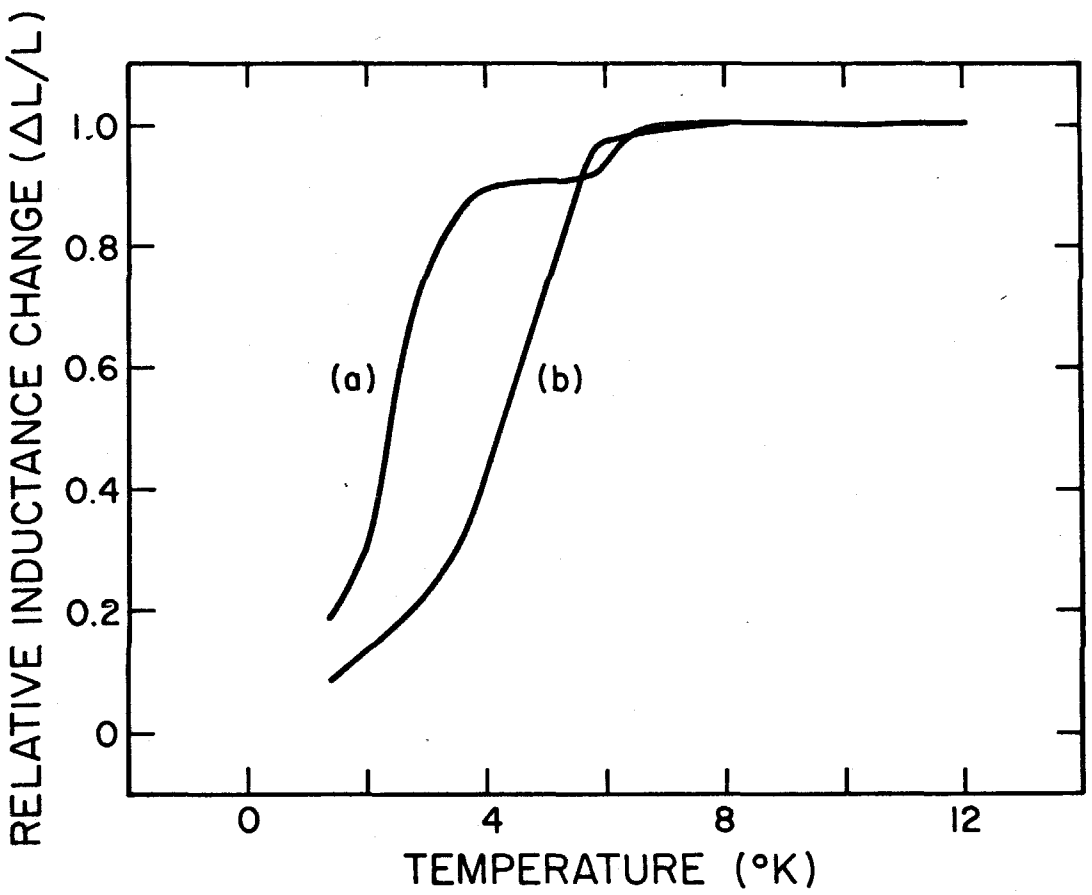

FIGURE 19. Relative Inductance Change as a Function of Temperature for (a) As-cast $Ga_{10}Ge_{90}$, and (b) Liquid-Quenched $Ga_{10}Ge_{90}$.

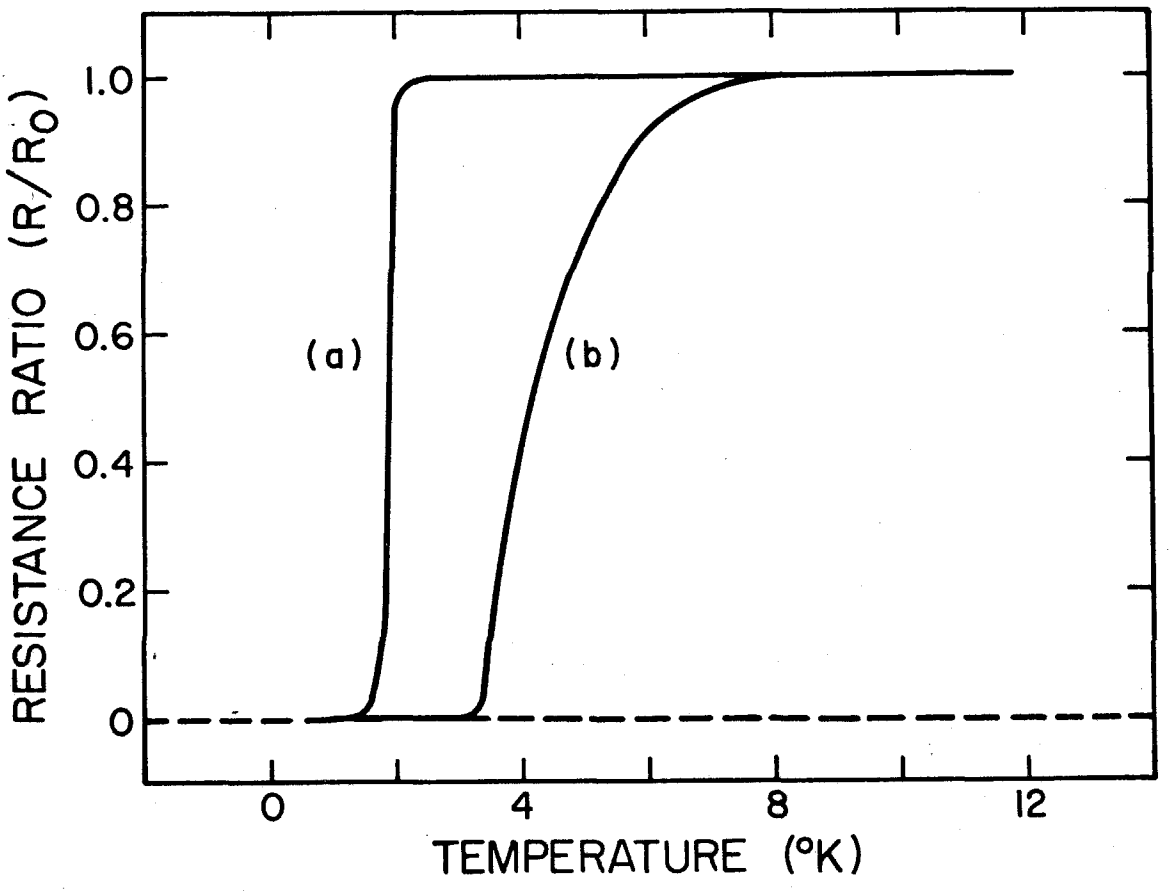

FIGURE 20. Electrical Resistance Ratio (R/R_0) (R_0 = Residual Resistivity at $10^{\circ}K$) as a Function of Temperature for (a) Liquid-Quenched $Ga_{50}Ge_{50}$, and (b) Liquid-Quenched $Ga_{10}Ge_{90}$.

Unfortunately, it was impossible to ascertain the crystal structure(s) of the Ga phase(s) in these alloys due to the low melting temperature of Ga (29.8°C). X-ray results show the clear presence of a Ge phase, along with many poorly defined lines associated with the Ga phase. No superconductivity was observed in the as-cast Be-Si alloys down to 1.3°K. Electrical resistance as a function of temperature for two liquid-quenched Be-Si alloys is shown in Figure 21. These alloys, $Be_{45}Si_{55}$ and $Be_{25}Si_{75}$ show resistive-transitions with $T_c' \cong 9.0^{o}K$ and $T_c' \cong 4.0^{o}K$, respectively. Alloys containing 62 at.% Be also show transitions with $T_c' \cong 9.0^{o}K$; however, the transitions are much broader and incomplete in most cases. No transition was observed in alloys containing 90 at.% Be. A large variation in the resistive behavior among liquid-quenched Be-Si samples of the same composition was observed. This variation could arise as a result of differences in the cooling rate from the melt during the quenching process. Also, during quenching, significant oxidation of Be can occur. Debye-Scherrer films of liquid-quenched Be-Si alloys show the presence of a Be phase, a Si phase, and varying amounts of the oxide BeO. No obvious correlation between the presence of BeO and superconducting properties was observed. Oxidation during liquid-quenching and sample handling can not be easily controlled.

Liquid-quenched Pb-Ge and In-Ge alloys were found by x-ray analysis to contain only Pb and Ge, and In and Ge, respectively. No enhancement of the In transition temperature ($T_c = 3.41^{o}K$) was observed. A small enhancement effect was observed for Pb. Results of electrical resistance measurements for the liquid-quenched alloys $Pb_{70}Ge_{30}$ and

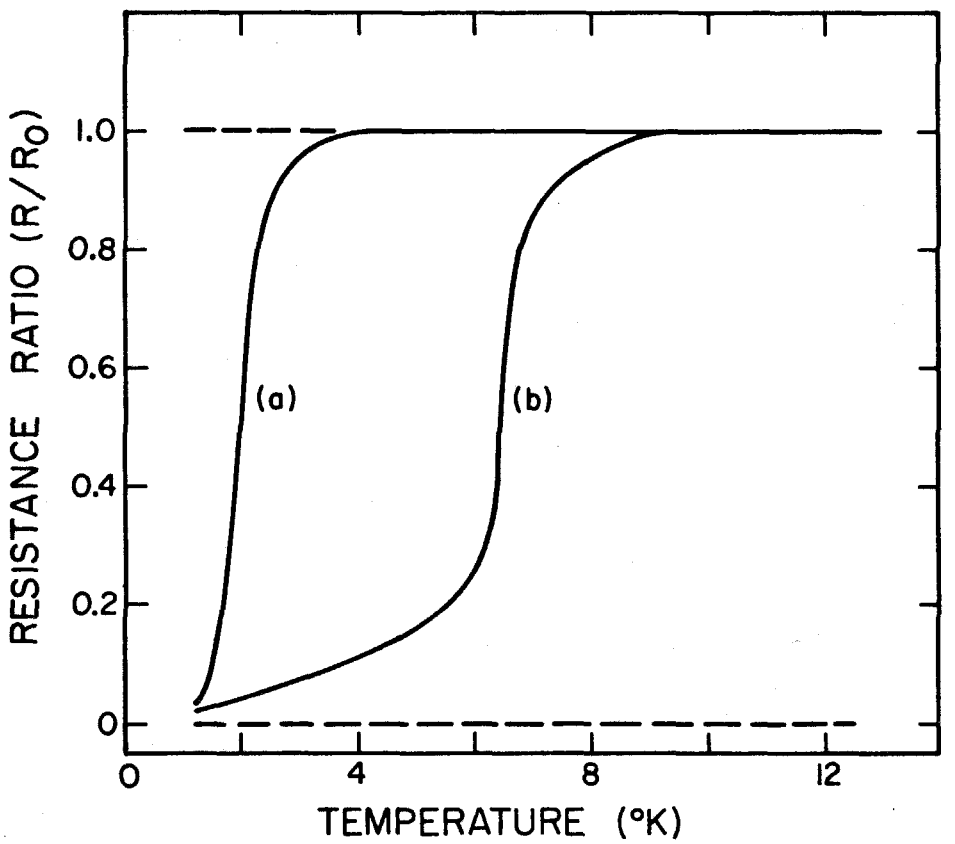

FIGURE 21. Electrical Resistance Ratio (R/R_0) (R_0 = Residual Resistance at 10^oK) as a Function of Temperature for (a) Liquid-Quenched $Be_{25}Si_{75}$, and (b) Liquid-Quenched $Be_{45}Si_{55}$.

$In_{70}Ge_{30}$ are shown in Figure 22. The Pb-Ge alloys containing less than 70 at.% of Pb showed a smaller enhancement effect.

To clarify the role of the semiconducting phase in the observed superconductivity of metal-semiconductor alloys, a study of the metal-metal Al-Al_2Cu eutectic was made. X-ray analysis of the as-cast alloy $Al_{48.1}$ $(Al_2Cu)_{51.9}$ (eutectic composition) indicated that only the phase Al and Al_2Cu were present. A metallographic study of the as-cast alloy shows that the microstructure consists of alternating lamellar domains of the two phases. A metallograph is shown in Figure 2(d). The characteristic domain size is noticeably smaller than that found in as-cast Al-Ge or Al-Si samples. Electrical resistivity measurements performed on the alloy show no evidence of a superconducting transition down to a temperature of $1.25^{o}K$.

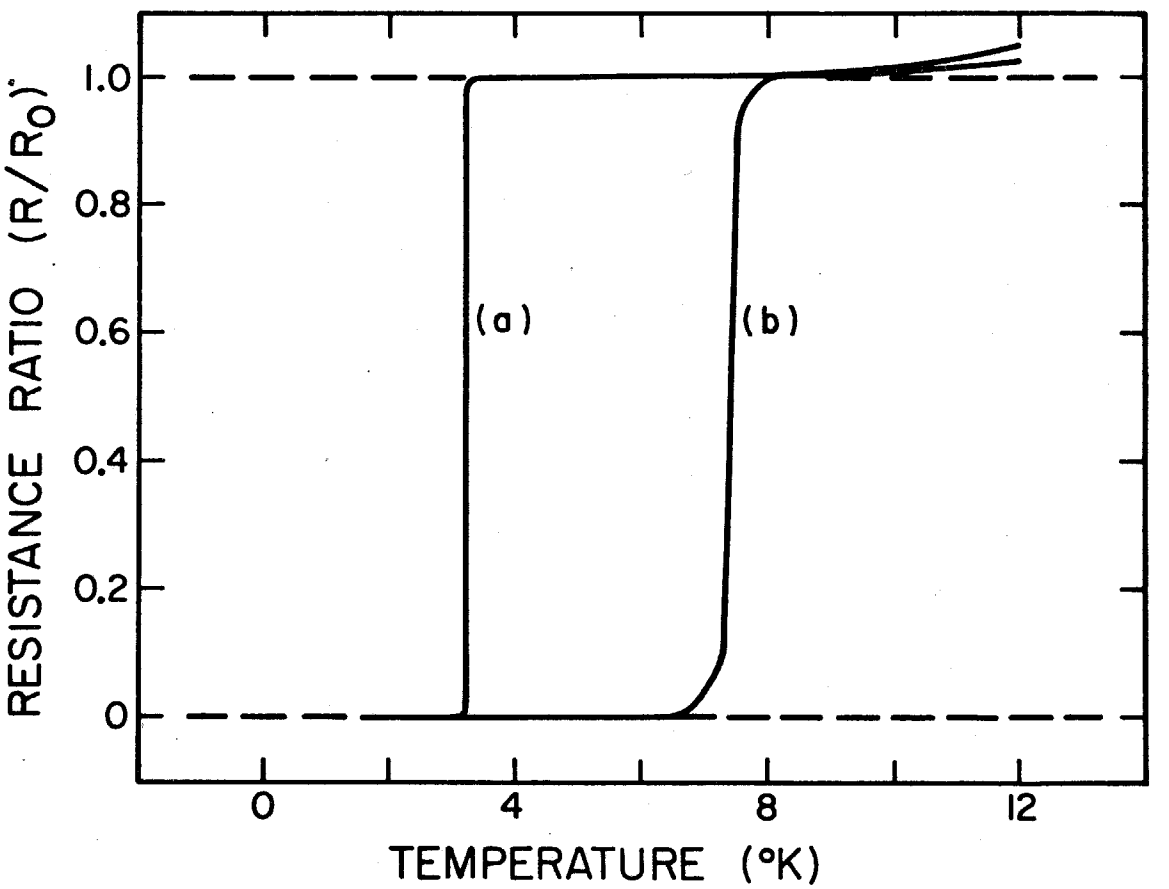

FIGURE 22. Electrical Resistance Ratio (R/R_0) (R_0 = Residual Resistance at 10^0K) as a Function of Temperature for (a) Liquid-Quenched $In_{70}Ge_{30}$, and (b) Liquid-Quenched $Pb_{70}Ge_{30}$.

IV. ANALYSIS AND DISCUSSION

A. Enhancement of Superconducting Transition Temperatures

The most interesting result of the present study is the observed enhancement of the superconducting transition temperature of the metallic component of the alloys. For reference, the superconducting transition temperatures of the pure metals are summarized in Table IV. The problem of explaining the observed enhancement of T_c for the alloys studied is not simple. Several factors, all of which may play a role in the superconductivity, deserve consideration. The following are among the most important.

1) The presence of dissolved Si or Ge in the metallic phase of an alloy, voids and defects in the metal lattice, and surface effects at the metal-semiconductor interface can result in softening of the phonon modes of the metal or a change in the electronic density of states at the Fermi level of the metal. As a result, the electron-phonon coupling constant λ may be altered and the superconducting transition temperature changed. McMillan (Reference 19), and others (Reference 20), have shown how this type of structural disorder can result in an enhanced superconducting transition temperature.

2) Quasi two-dimensional electronic states, localized at the metal-semiconductor interface, resulting in surface superconductivity could be considered. Ginzburg (References 1 and 21) has proposed and discussed this type of superconductivity.

3) In liquid-quenched alloys, new crystalline phases which are metastable may be formed. The presence of such a metastable phase in the alloys could explain the enhanced superconducting transition temperature.

4) The high onset temperature T_c' in some alloys (e.g., 7.5^oK for Al-Si and 9.0^oK for Be-Si) may result from superconducting fluctuations of a Curie-Weiss nature, rather than a true superconducting state.

5) If electrons near the Fermi surface of the metal can tunnel a significant distance into adjacent semiconducting domains, then an exciton mechanism such as that proposed by Allender, Bray and Bardeen (Reference 2) could be effective in enhancing the transition temperature of the metal.

These five possible explanations for the enhanced superconductivity of the alloys may not be inclusive; but, the list covers most of the mechanisms for enhancement discussed in the literature. An analysis of each possibility is now given to determine which, if any, are important in understanding the experimental results of this study.

1) Owing to its nearly free electron behavior, the metal Al has an electronic density of states near the Fermi level, which is quite insensitive to disorder. Experimental studies of the Al band structure (Reference 22) indicate free electron approximation for the density of states $N(E) \sim E^{\frac{1}{2}}$ gives a rather good description of the actual band structure. The introduction of defects, voids, or substitutional impurities in the Al matrix tends to reduce the electronic mean free path and leads to subsequent broadening of electronic energy levels. Details in the structure of $N(E_F)$ are lost. (Reference 23.)

In the limit of extreme disorder, the free electron approximation is reasonably good for the ordered material. Thus, disorder should have little effect on the behavior of N(E). According to the McMillan theory of superconductivity (Reference 19), the superconducting transition temperature of an Al-base alloy having the f.c.c. (face centered cubic) structure of pure Al should be principally determined by the McMillan average squared phonon frequency:

$$\langle \omega^2 \rangle_M = \left[\frac{\langle \omega \rangle}{\langle 1/\omega \rangle} \right] \tag{1}$$

where $\langle\ \rangle$ denotes average over the entire phonon spectrum. The McMillan theory can be best applied to cases where the electronic density of states N(E) is a slowly varying function of energy making it very suitable for the present problem. McMillan (Reference 19) derives the expression:

$$T_c = \frac{\Theta_D}{1.45\ e^{\left\{1.04(1+\lambda)[\lambda+\mu^*(1+0.62\lambda)]^{-1}\right\}}} \tag{2}$$

for the superconducting transition temperature of an alloy. In the formula, λ is the electron-phonon coupling constant, μ^* is the renormalized Coulomb interaction constant, and Θ_D is the Debye energy of the material. For a free electron metal, McMillan shows that λ can be related to several fundamental parameters by the expression:

$$\lambda = \frac{1.51}{r_s} \left[\frac{\langle y_q^2 \rangle}{(\langle \omega^2 \rangle_M / \Omega_p^2)} \right] \tag{3}$$

where r_s is the radius in Bohr radii of a sphere containing one electron. The quantity $\langle V_q^2 \rangle$ is a dimensionless average of the electron psuedopotential matrix element squared, and Ω_p^2 is the ionic plasma frequency of the metal. McMillan argues that for simple metals, the important contribution to λ comes from variations in $\langle \omega^2 \rangle_M$. Thus, λ is roughly proportional to $1/\langle \omega^2 \rangle_M$ for a given class of materials (e.g., f.c.c. Al-base alloys). It can be seen that a decrease in λ can lead to an increase in T_c. McMillan uses a simplified expression containing the essential dependence of T_c on $\langle \omega^2 \rangle_M$:

$$T_c = \langle \omega \rangle e^{-[(M\langle \omega^2 \rangle_M / C) - 1]} \qquad (4)$$

to show that a maximum value of T_c for a given class of materials exists. In Equation (4), M is the mean atomic weight of the constituent atoms in the alloy, and C is a constant which can be determined given the value of λ and $\langle \omega^2 \rangle_M$ for one member of the class from $\lambda = C/M\langle \omega^2 \rangle_M$. The maximum value of T_c is obtained for $\lambda = 2$ as $\langle \omega^2 \rangle_M$ is varied.

Strongin (Reference 8) has used Equation (1) and the value $\lambda_{Al} = 0.38$ estimated by McMillan for pure Al to argue that a decrease of 30% in Θ_D^2 can account for the maximum transition temperature ($T_c = 5.7^{\circ}K$) obtained for ultrathin Al films evaporated on a cryogenic substrate. Strongin assumes that $\langle \omega^2 \rangle_M$ is proportional to Θ_D^2. Paskin and Dickey have performed computer calculations using molecular dynamic techniques to simulate the phonon spectrum of a thin film. (Reference 24.) They found that a reduction of 25% in $\langle \omega^2 \rangle_M$ could be expected for a model Al disk consisting of 166 atoms arranged in three

layers with one free surface. As the thickness of the model disk is increased, the value of $\langle\omega^2\rangle_M$ rapidly returns to that of bulk Al. Dickey and Paskin conclude that phonon mode softening is primarily due to free surface area, and thus depends on the surface-to-volume ratio of the model disk. According to Dickey and Paskin, Strongin, and others (Reference 25), a significant change in $\langle\omega^2\rangle_M$ for bulk material is expected only when the material density changes; that is, when voids, defects, and large internal surface areas are present in a material, as could be the case in granular films with small grain size.

In the case of liquid-quenched Al-Si alloys, a large density change would be required to account for the observed $T_c \cong 5.7^oK$. Strongin (Reference 23) assumes that $\Theta_D = CV^{-\gamma}$, where C is a constant for a given metal, V the volume of the metal, and γ is the Gruneisen constant for the metal. For Al, $\gamma \cong 2$, and thus the 30% change in Θ_D^2 implies a change in volume of $\sim$ 15% and a similar change in density. This might occur for a granular cryogenic film (Reference 26), but for an alloy obtained from the liquid state, it is not possible. Such a density change is at least three times that observed during melting of any alloy. Unlike the case of granular films obtained by vapor deposition on a cryogenic substrate, the liquid-quenched Al-Si alloys do not have large free internal surface area. It is difficult to account for a large change in $\langle\omega^2\rangle_M$ based on the preceding approach. The case of liquid-quenched Be-Si alloys would be considerably more difficult since even larger density changes would be required ($T_{c0} = 0.01^oK$ and $T_c' \cong 9^oK$). It should be pointed out that recent tunneling experiments

on cryogenically deposited granular Al-Ge films have failed to substantiate claims of phonon mode softening. (Reference 28.) In summary, it is unlikely that large density changes can account for the enhancement of T_c observed in the present case. If disorder and phonon mode softening is responsible for the present enhancement effect, it must be viewed in another way.

Recent experiments performed by the author on transition metal alloys suggest a relationship between the features of the phase diagram of an alloy and the problem of phonon mode softening and its significance for superconductivity. (Reference 27.) It is interesting to apply these results to the present case.

The basic idea behind this approach is to relate changes in the melting temperature of an alloy, as described in the liquidus curve in the phase diagram, to corresponding changes in $\langle\omega^2\rangle_M$. The approach may be applied to phases which exist over a broad homogeneity range, or can be obtained over an extended non-equilibrium homogeneity range through, for example, liquid-quenching. The motivation behind this approach is provided by the observation that the frequency of phonon modes is related to the bonding characteristics of the constituent atoms in an alloy phase. Substitutional Si in a f.c.c. Al matrix, for example, reduces the cohesive energy of the lattice by raising the total energy of the electron-lattice system. In the limit of high Si impurity concentration, the f.c.c. structure becomes unstable and can no longer exist. The characteristic phonon frequencies of the lattice are progressively lowered as this limit of instability is approached. This reduction in phonon frequencies is not accompanied

by a decrease in density. The lattice parameter of the matrix actually decreases with increasing content of dissolved Si (see Figure 11).

The melting temperature of pure Al is 660°C. The temperature of the liquidus curve in the phase diagram (Figure 1) is seen to decrease with addition of Si to the alloy, reaching a minimum at the eutectic composition $Al_{89}Si_{11}$ of 577°C. This represents a fractional change of 0.09 in T_M, the melting temperature of the alloy in °K. This must be related to a fractional change in the Debye energy, or $\langle\omega^2\rangle_M$, for comparison to the McMillan theory. Since a good microscopic theory of melting does not exist, the Lindemann relation (Reference 29) is used as a first approximation to the relation between T_M and Θ_D. The Lindemann relation can be derived from fundamental considerations. Wilsdorf (Reference 30), for example, has shown that the relation can be derived from a theory of melting based on the free energy for formation of glide dislocations in a crystal. The Lindemann relation is expressed as:

$$\Theta_D^2 = \frac{CT_M}{V^{2/3}} \tag{5}$$

where C is a constant for a given material reciprocally related to the mean atomic weightsof the constituent atoms. Since the atomic weights of Al and Si (26.98 and 28.01) are almost equal, we will ignore variations in C. The parameter V is the mean atomic volume which also is nearly constant since the fractional change in Al lattice parameter is less than 0.001 in the Al-Si alloys. Thus, T_M can be expected to give a reasonable representation of Θ_D^2. A fractional change of 0.09 in T_M will result in the same fractional change in Θ_D^2. Taking $\langle\omega^2\rangle_M \sim \Theta_D^2$,

one can estimate the behavior of T_c. With $\lambda \sim 1/\Theta_D^2$ and an initial value of $\lambda_{Al} = 0.38$ calculated by McMillan for pure Al, the approximate behavior of T_c described in Equation (4) predicts that a fractional decrease of 0.09 in Θ_D^2 results in an increase from $T_c = 1.18^oK$ to $T_c \cong 1.45^oK$. An initial value of $\lambda_{Al} = 0.30$ for pure Al gives the observed $T_c = 1.55^oK$ for as-cast Al-Si alloys. The above analysis applies to the Al phase present in an equilibrium alloy at the eutectic composition $Al_{89}Si_{11}$. In particular, it describes the Al phase present in an alloy at the eutectic composition well-annealed just below the eutectic temperature (577^oK) since the melting of this alloy is the basis for defining the fractional change in T_M. In both the as-cast and well-annealed (at 500^oC) $Al_{90}Si_{10}$ alloys, the observed superconducting transition temperature is 1.55^oK. For Al-Ge alloys, the eutectic composition is $Al_{70}Ge_{30}$ and $T_M = 424^oC$, which represents a fractional change of 0.25 compared to pure Al. With $\lambda_{Al} = 0.38$, T_c is predicted (from Equation (4)) to be 1.9^oK. For $\lambda_{Al} = 0.30$, $T_c = 2.2^oK$. As-cast and well-annealed (at 300^oC) samples of $Al_{70}Ge_{30}$ have an observed $T_c = 1.85^oK$ and $T_c' = 2.2^oK$. The agreement with the preceding estimates is quite good.

It is now necessary to examine the phase diagram in more detail. The Al phase described in the preceding argument is that obtained at the eutectic composition on freezing of the alloy. This phase coexists with a pure Si (Ge) phase (the solubility of Al in Si (Ge) is negligibly small). According to the phase diagram (Reference 9), this Al phase contains 1.6 at.% Si (2.8 at.% Ge) in solid solution. Θ_D^2 is reduced by 10% for this phase. Assuming that (at least locally) Si is

retained in solid solution by liquid-quenching up to the eutectic composition of 11 at.% Si in Al, we can estimate (using linear extrapolation) the effect on Θ_D^2 for an Al-base f.c.c. solid solution with composition $Al_{89}Si_{11}$. The fact that the eutectic composition should be taken as a natural limit for extension of terminal solubility has been discussed in the literature (References 31 and 32). Linear extrapolation gives a fractional change of 0.68 in Θ_D^2 for a metastable solid solution containing 11 at.% Si. Equation (4) with $\lambda_{Al} = 0.38$ then predicts $T_c = 4.2^oK$. With $\lambda_{Al} = 0.30$, $T_c = 7.2^oK$ for this metastable solid solution. If Si is dissolved in the Al phase of liquid-quenched alloys up to 11 at.% in regions where the cooling rate is greatest (near the substrate) and somewhat lesser amounts elsewhere, then the observed maximum $T_c = 5.7^oK$ and $T_c' = 7.5^oK$ would be very consistent with the above estimates. The values of $\lambda_{Al} = 0.38$ calculated by McMillan, and $\lambda_{Al} = 0.30$ have both been used above. Some uncertainty exists in this parameter and both values are used to show how the estimates of T_c depend on it. The value 0.30 gives the best consistent fit to the results.

In addition to predicting the maximum T_c obtainable (by extension of the solubility to the eutectic composition) for the Al base f.c.c. solid solution, one can also predict the behavior of T_c for solid solutions containing less Si. This has been done and the results (with $\lambda_{Al} = 0.38$ and 0.30) are given in Table V for comparison with the observed transition temperature of liquid-quenched Al-Si alloys containing less than 11 at.% Si (hypoeutectic alloys) and those with greater than 11 at.% Si (hypereutectic alloys). Of course, Si is

Alloy	Predicted T_c (^oK)		Observed T_c and T_c' (^oK)
	$\lambda = 0.30$	$\lambda = 0.38$	
Al		1.18	1.18
Al_1Si_{99}	1.30	1.25	<1.3, <1.3
$Al_{2.5}Si_{97.5}$	1.75	1.55	1.3, 1.5
Al_5Si_{95}	2.65	2.15	1.7, 2.4
$Al_{10}Si_{90}$	5.65	3.70	2.2, 3.9
$Al_{15}Si_{85}$	7.20	4.20	3.3, 5.1
$Al_{20}Si_{80}$	7.20	4.20	4.0, 6.0
$Al_{25}Si_{75}$	7.20	4.20	5.6, 6.2
$Al_{30}Si_{70}$	7.20	4.20	5.5, 6.5
$Al_{40}Si_{60}$	7.20	4.20	4.0, 7.5

TABLE V. Predicted Values of T_c Using McMillan Approach for an f.c.c. Solid Solution of Si in Al With $\lambda_{Al} = 0.30$ and $\lambda_{Al} = 0.38$ Compared to Observed Transition Temperatures of Al-Si Alloys. It Is Assumed that the Si Content of the Solid Can Not Exceed 11 at.%.

completely dissolved only when the Si content of the alloy is less than $\sim$ 5 at.% as evidenced by formation of Si precipitate for greater Si concentrations. More Si-rich solid solutions ($\sim$ 11 at.%) may be obtained in local regions near the substrate in hypereutectic alloys. The fact that Si precipitates in much larger quantity near the substrate (see Figure 3) in such alloys provides evidence for this view.

Applying the preceding analysis to Al-Ge alloys yields a higher estimate of T_c ($\sim 8^oK$) than that observed if it were assumed that an f.c.c. solid solution could be obtained up to the eutectic composition of 30 at.% Ge. It is observed that new metastable crystalline phases form when the Ge content of liquid-quenched Al-Ge alloys exceeds about 15 at.%. (References 16 and 17.) It appears that T_c is limited to about 6^oK for the Al-base f.c.c. solid solution with Ge by the intrinsic instability of this phase. This instability leads to the formation of non-equilibrium crystalline phases in the Al-Ge system. It is energetically unfavorable for Ge to dissolve in Al up to the eutectic composition of 30 at.% Ge. The free energy of the metastable phases is lower than that of the super-saturated f.c.c. solid solution of Ge in Al.

The annealing behavior of liquid-quenched Al-Si alloys can also be understood in terms of the above analysis. An f.c.c. solid solution containing 11 at.% Si was characterized by a fractional decrease at 0.68 in Θ_D^2. This implies that the "effective" melting temperature of this solid solution is roughly $0.32\ T_{MO} \cong 300^oK$. That is, the solid solution is unstable at this temperature and will decompose into a less Si-rich solid solution plus a Si phase. For observed alloys

with $T_c \cong 5.7^oK$ an "effective" melting temperature of $0.39T_{MO} \cong 360^oK$ is estimated from Equations (4) and (5) with $\lambda_{Al} = 0.30$. These predictions are consistent with the fact that only traces of superconductivity above $\sim 6^oK$ are observed in liquid-quenched hypereutectic Al-Si alloys handled at room temperature. Furthermore, it is consistent with the observed decrease in T_c to $\sim 3^oK$ after annealing at 100^oC for one hour, and the decrease to $\lesssim 2^oK$ after annealing at 300^oC for one hour. It further implies that were these alloys quenched and maintained on a low temperature (liquid nitrogen cooled) substrate, then a bulk T_c near 7^oK could be obtained. Unfortunately, the samples cannot be prepared and maintained during handling at this temperature, so it is not possible to test this prediction.

A brief discussion of the enhancement effect in Sn-Ge, Pb-Ge, and Be-Si alloys in terms of the preceding approach is now presented for completeness. The equilibrium phase diagrams for Pb-Ge and Sn-Ge are very similar. Both show a eutectic composition containing < 1 at.% Ge in the metal. (References 33 and 34.) The solubility of Ge in both metals at the eutectic temperature is less than 0.1 at.%; however, both Pb-Ge and Sn-Ge alloys exhibit mutual solubility of the constituents in the liquid state. The lack of significant solid solubility in equilibrium and the close proximity of the eutectic composition to the pure metal make an analysis based on the relation between solubility and melting temperature, as was done for Al-base alloys, infeasible. Lattice parameters for the Pb and Sn phases of the liquid-quenched alloys are within experimental error identical to those of the pure metals. No indication of the degree of terminal solubility extension can be obtained

from these facts. The values of T_c' are enhanced in these cases, whereas the bulk transition temperature remains nearly identical to that of the pure metals. Thus, extended solubility of Ge in the metals may occur only in local regions near the substrate, and x-ray analysis of the entire sample would fail to detect significant changes in the lattice parameters of the Pb and Sn phases. Explaining the enhancement effects for these alloys ($T_c' = 6.5^oK$ for Sn-Ge and $T_c' = 7.8^oK$ for Pb-Ge) requires a smaller degree of phonon mode softening than required in the case of Al-base alloys. If one takes $\lambda_{Pb} = 1.12$ and $\lambda_{Sn} = 0.60$ as estimated by McMillan for the pure metals, then a decrease of 5% and 45% in Θ_D^2, respectively, explains the maximum observed enhancement of T_c based on Equation (4). It is worthwhile to note that the McMillan theory predicts a maximum T_c of $\sim 7^oK$ for a Sn-base alloy and $\sim 9^oK$ for a Pb-base alloy. These predictions are consistent with the maximum observed enhancements in this study.

The case of Be-Si alloys is much more difficult to explain in terms of phonon mode softening. For liquid-quenched $Be_{45}Si_{55}$ with $T_c' = 9^oK$, a fractional change in Θ_D^2 of $\sim 70\%$ is required. The atomic radius of Si ($r_{Si} = 1.32$ A) is much larger than that of Be ($r_{Be} = 1.12$ A). According to Hume-Rothery (Reference 35), this should result in very restricted mutual solubility. No change in the lattice parameter of the Be phase was detected by x-ray analysis. It is unlikely that the presence of dissolved Si in Be can account for a change of 70% in Θ_D^2. Alloy work on Be shows that small amounts of certain transition metals can raise the T_c of Be to $\sim 9^oK$. For example, $Be_{22}Re$ has $T_c = 9.6^oK$ and the electronic density of states at the Fermi level is three times

that of pure Be. (Reference 36.) In pure Be, the Fermi level misses the peak in N(E). It is possible that small amounts of Si in a Be matrix along with disorder introduced by liquid-quenching could significantly alter $N(E_F)$. This could result in a large enhancement of T_c. No evidence was found for a structural change in the Be phase of liquid-quenched Be-Si alloys; but, the fact that the superconducting transition observed in these alloys is incomplete implies that only a limited amount of a metastable phase along the grain boundaries could explain the observed superconductivity. Since Be has a very low x-ray scattering power (scattering power is proportional to Z^2), it would be difficult to detect such a phase. In summary, the case of liquid-quenched Be-Si alloys is more complex than that of Al-Si alloys and cannot be explained simply in terms of phonon mode softening.

2) Although Strongin has shown that Al films may be grown epitaxially on a single crystal of Si (Reference 6), it is unlikely that the Al-Si interface in the present alloys is a coherent one. It seems likely that an incoherent interface characterized by a varying amount of surface electronic charge is present in the Al-Si eutectic. The possibility that surface electronic states localized at the interface regions participate in some type of surface superconductivity cannot be readily ruled out; however, there is the objection that long range order cannot exist in a two-dimensional system as discussed by Ginzburg (Reference 1) and others.

3) The possibility that a third undetected metastable phase exists in the as-cast alloys is remote. For the liquid-quenched alloys, magnetization measurements, and electrical resistivity measurements

indicate that the superconductivity is a bulk property of the alloys. That a third phase undetected in the x-ray analysis could account for this is unreasonable.

4) Strongin (Reference 37) and others (Reference 38) have pointed out that fluctuation behavior of a Curie-Weiss nature can occur in thin films when the electronic mean free path is small. The high onset temperature T_c' of liquid-quenched Al-Si, Be-Si, and Sn-Ge may be associated with such behavior. Examination of Figure 11(b) suggests, for example, that the portion of the resistive transition above $\sim 5.7^{o}K$ has the characteristics of fluctuation phenomenon. Using the free electron model, and the estimated value of 10^{-4} Ωcm (Section III) for the residual resistivity of liquid-quenched $Al_{70}Si_{30}$, one can estimate the electronic mean free path (the residual resistivity is difficult to calculate exactly due to the non-uniform nature of the samples). An estimate of $\sim 5\text{Å}$ is obtained for the mean free path. In this case, superconducting fluctuations above T_c might be expected. Comparison of the results of Figure 11(b) with those reported by Strongin for granular Al films with a mean free path of 5Å shows a marked similarity. Thus, care should be exercised when defining the highest temperature for which a stable superconducting state exists in these alloys. T_c' may not represent a true transition temperature for some alloys.

5) Of the metals studied, enhancement of T_c was observed for Al, Be, Ga, Sn, and Pb. No significant enhancement was observed for the metals In and Tl. If the maximum observed enhancement $(T_c' - T_{c0}) = (\Delta T_c)_{max}$ for each of the metals is plotted as a function of the Fermi

energy calculated using the free electron model, then a systematic trend appears. This is illustrated in Figure 23. For Al, $(\Delta T_c)_{max}$ is nearly the same for both Al-Ge and Al-Si alloys; but, since the presence of a metastable phase in Al-Ge alloy plays a role in the superconductivity (References 16 and 17), the maximum enhancement for Al-Si alloys is plotted. For other metals, $(\Delta T_c)_{max}$ is taken to be the result obtained in a Ge matrix. Only the result for the dominant transition at $3.5^{o}K$ is used for Ga-Ge since the presence of β Ga is likely to be responsible for the small transition at $6.4^{o}K$. It is seen that enhancement occurs only when the Fermi energy of the metals exceeds a minimum "threshold" value. This value is about 9-10eV. The enhancement effect increases consistently as the Fermi energy of the metal increases above this "threshold" value. The Allender, Bray, Bardeen (Reference 2) model for an exciton mechanism predicts this type of behavior. The present results are now discussed in terms of this mechanism.

Consider a simple model for the Al-Si and Al-Ge microstructure consisting of alternating lamellar domains of Al and Si(Ge) of thickness t_{Al} and t_{Si}, respectively. Consider, in particular, a single Al domain sandwiched between Si layers as shown in Figure 24. Electrons near the Fermi level of Al presumably tunnel a distance D into the Si domains and interact with the covalently bound electrons of the Si valence band. The exchange of virtual excitons by these tunneling electrons leads to an attractive interaction in much the same way that the exchange of phonons leads to attraction in the conventional BCS theory. ABB gives the superconducting transition temperature of such a sandwich configuration by the following approximate formula:

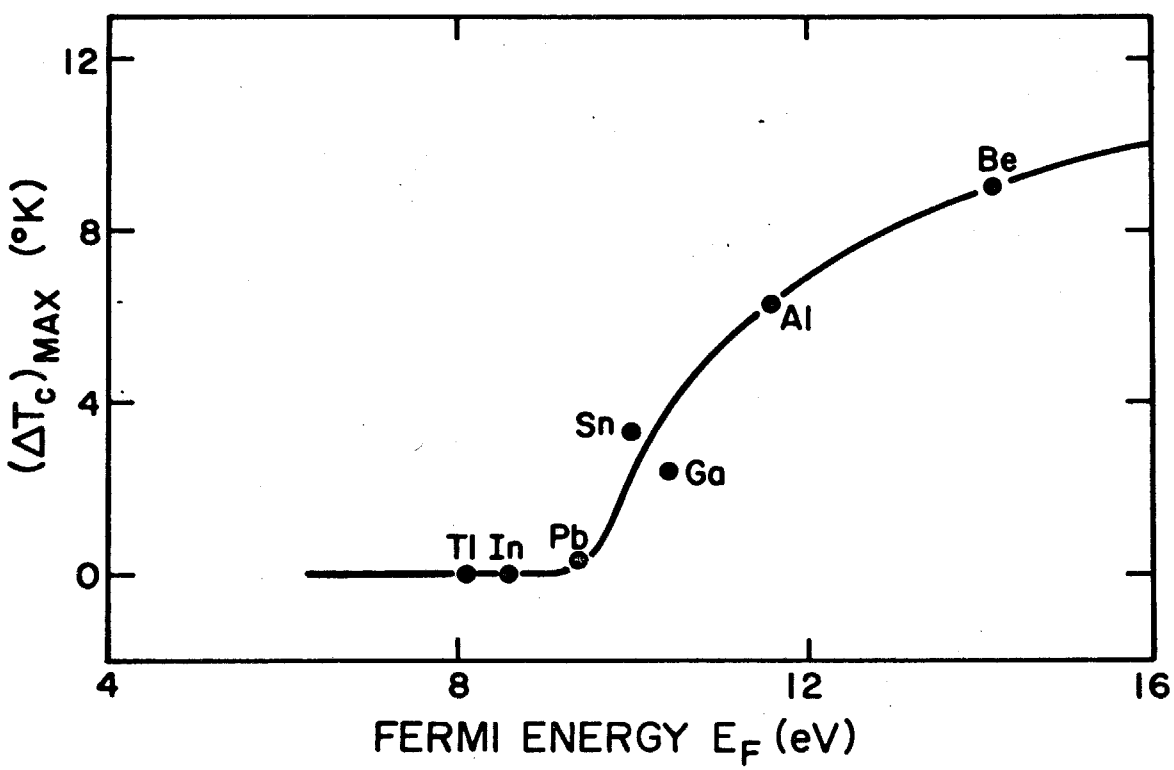

FIGURE 23. Maximum Observed Enhancement of T_{c0} (Bulk Metal Transition Temperature) as a Function of Fermi Energy Calculated From Free Electron Model for Various Metals in this Study.

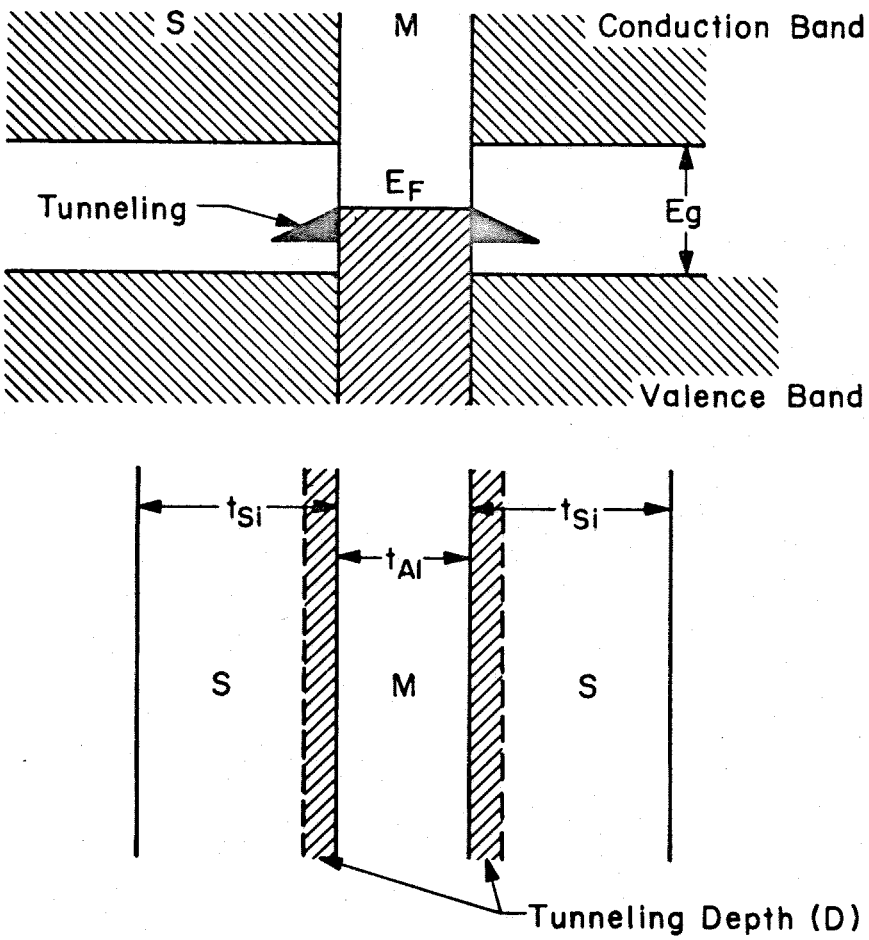

FIGURE 24. Illustration of the Metal-Semiconductor Domain Geometry Used in Applying the ABB Model. In the Diagram, M Refers to the Metal (Al) Domain and S to the Semiconducting (Si) Domain.

$$T_c = \frac{\Theta_D}{1.45} e^{(-1/geff)} \tag{6}$$

$$geff = \frac{\lambda^*_{ph} + (\lambda^*_{ex} - \mu')}{1 - (\lambda^*_{ex} - \mu')\ln\left(\frac{\omega_g}{\omega_{po}}\right)} \tag{7}$$

$$\mu' = \frac{\mu}{1 + \mu\ln\left(\frac{\omega_F}{\omega_g}\right)}$$

The parameters λ^*_{ph} and λ^*_{ex} are the renormalized phonon and exciton interaction constants; μ is the Coulomb interaction constant; $\hbar\omega_g$ and $\hbar\omega_F$ are the average energy gap of the semiconductor and the Fermi energy of the metal, respectively; and Θ_D and $\hbar\omega_{po}$ are the Debye temperature and energy of the metal, respectively. This is applied to the present case by requiring that $T_c = 1.18^oK$ (the transition temperature of bulky Al) when $\lambda^*_{ex} = 0$. Taking $\hbar\omega_F = 11.6eV$ for Al (free electron model) $\hbar\omega_g = 1eV$, $\Theta_D = 428^oK$ and a reasonable estimate of $\mu = 0.3$ for Al). Then it is found that $\lambda^*_{ph} = 0.29$ for bulky Al. Now for a given enhancement of T_c, an estimate can be made for λ^*_{ex}. In Figure 25, a plot is shown which shows how T_c depends on λ^*_{ex} for the given choice of relevant parameters. In particular, if $T_c = 1.8^oK$ and $T_c = 5.7^oK$, then $\lambda^*_{ex} = 0.034$ and $\lambda^*_{ex} = 0.127$, respectively. The corresponding unrenormalized values of the exciton interaction constant ($\lambda_{ex} = \lambda^*_{ex}/\{1 - \lambda^*_{ex}\}$) are $\lambda_{ex} = 0.035$ and $\lambda_{ex} = 0.161$. Using the ABB approximate expression for λ_{ex} in terms of the characteristic parameters of the sandwich:

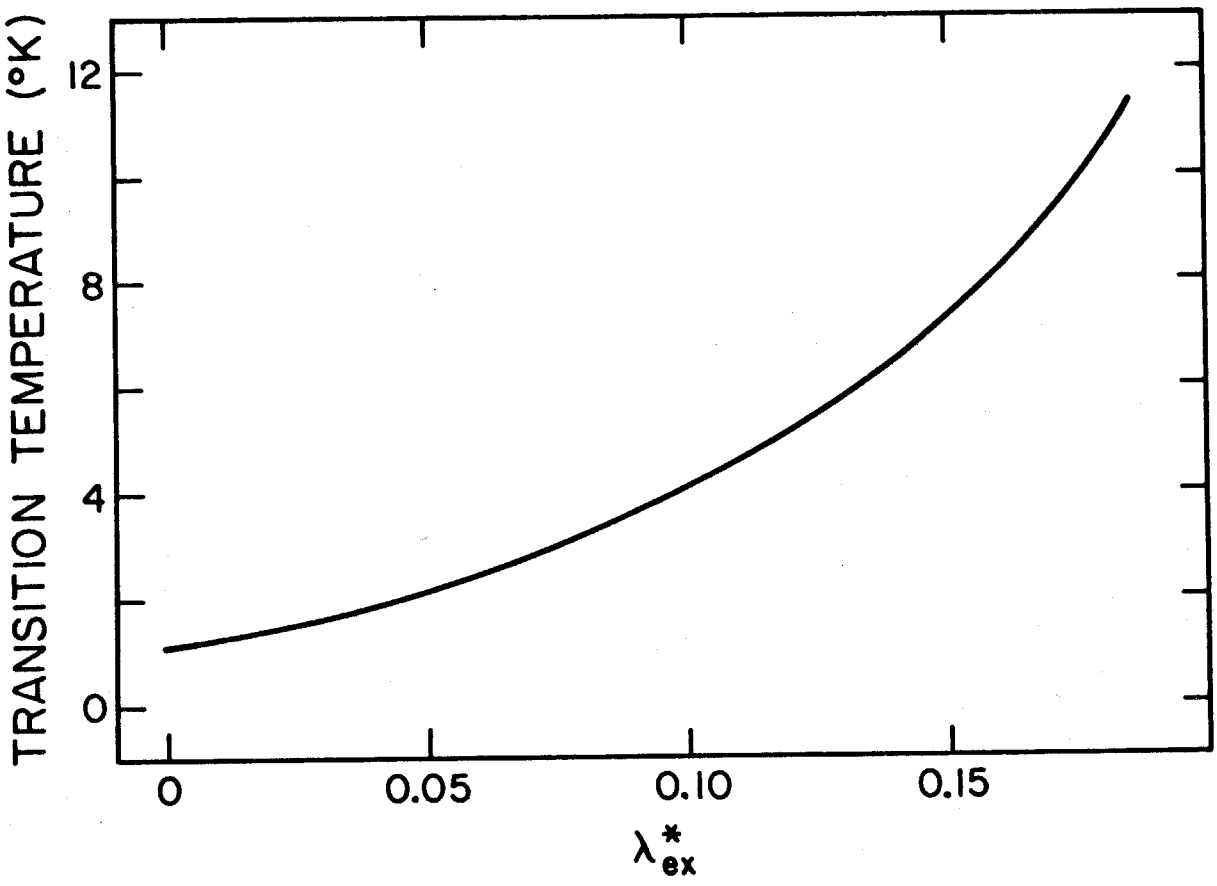

FIGURE 25. The Dependence of the Superconducting Transition Temperature of an Al Domain on the Exciton Coupling Strength λ^*_{ex} Calculated from the ABB Model.

$$\lambda_{ex} \cong s\gamma b\mu\left(\frac{\omega_p^2}{\omega_g^2}\right) \tag{9}$$

a rough idea of the value of these parameters is obtained. In the formula, $\hbar\omega_p$ is the plasma frequency of the valence electrons of the semiconductor calculated from the free electron model. A screening factor s approximates the effect of the dielectric tensor ($s \sim \frac{1}{\varepsilon}$), and γ is a factor which accounts for the exponential decay of the metal electron wave functions which represent tunneling into the semiconductor regions. The factor b, is the fraction of time which a metal electron spends in the semiconductor region. This factor is taken to be of order $(\gamma(2D)/t_{Al})$ where D is the tunneling depth and the factor of 2 arising from the semiconductor being on both sides of the metal. Taking $\hbar\omega_g$ = 1eV and $\hbar\omega_p$ = 10eV, and assuming the estimates of $S \sim \frac{1}{3}$ and $\gamma \sim \frac{1}{3}$ one finds that λ_{ex} = 0.035 (T_c = 1.8°K) and λ_{ex} = 0.161 (T_c = 5.7°K) give respectively b ∿ 0.012 and b ∿ 0.048. Then taking the value of $T_{Al} \sim 1000\text{Å}$ as observed in SEM studies of as-cast $Al_{70}Ge_{30}$, one finds $D \gtrsim 17\text{Å}$. Letting the average value of $t_{Al} \sim 200\text{Å}$ for liquid-quenched $Al_{70}Si_{30}$ gives $D \sim 14\text{Å}$. The values of D represent a lower bound for this parameter since other unknown parameters (γ, s) have been assigned favorable values. All of this information is summarized in Table VI.

The above estimates for D are very rough; however, one fact emerges from them: To account for the observed enhancement effect, a somewhat larger value of D than that indicated by ABB must be assumed. ABB estimate that $D \sim 5\text{Å}$, whereas the present results require $D \gtrsim 15\text{Å}$.

T_c (^oK)	λ_{ex}	b	t_{Al} (Approx.) (Å)	D ($\gtrsim$) (Å)
1.8	0.005	0.012	1000.	17
5.7	0.161	0.048	200.	14

TABLE VI. Approximate Values for λ_{ex}, b, t_{Al}, and D for a Given Al Transition Temperature T_c. Values of $\gamma \sim 1/3$, $S \sim 1/3$, $\hbar\omega_p = 10eV$, $\hbar\omega_g = 1eV$, and $\mu = 0.3$ Were Assumed.

Concerning this fact, the following points should be noted. First, in the alloys studied here, the Si and Ge phase are probably very heavily doped with p-type Al impurities. The presence of these impurity levels in Si (Ge) might be essential for obtaining an increased tunneling depth D. Second, it is likely that the Al-Si interface in the alloys is of the incoherent type. This lack of coherence could result in surface conditions which are favorable to tunneling and thus, to the electron-exciton interaction. Strongin, et al., have recently reported results for ultrathin Al films epitaxially deposited on a single Si crystal. (Reference 6) No significant enhancement of T_c was found. The lack of p-type impurities in the Si along with the fact that a coherent interface is formed are possibly important in accounting for the differences between the present results and those of Strongin. Also, for ultrathin Al films ($\sim$10-50Å), the effect of extremely small dimensions on the electronic structure, particularly the electron density of states at the Fermi level, plays an unclear role in the exciton mechanism.

The results shown in Figure 23 suggest that the observed enhancement effect depends on the Fermi energy of the metal involved. Numerical calculations by ABB predict the functional dependence of T_c on E_F (Figure 7 of Reference 2 illustrates this dependence) when other relevant parameters are fixed. In particular, ABB predict that T_c will be a rapidly increasing function of E_F. Also, the results of ABB show that no significant enhancement should be observed below a "threshold" Fermi energy which is determined by the other fixed parameters (i.e., μ, ω_g, λ, and A = width in energy units of the exciton spectrum). The

behavior observed in Figure 23 with an apparent "threshold" of $E_F \sim 10eV$ is at least consistent with the predictions of ABB. Some typical results obtained by ABB using numerical computer methods are shown in Figure 26 for comparison with Figure 23.

B. Magnetic Properties

Up to this point, the discussion has dealt only with the mechanism behind the enhancement effect. Nothing has been said regarding the observed magnetic properties of the alloys. It is important to analyze this aspect of the problem. The magentic behavior expected from a microscopic array of metal and semiconductor domains will be complex. Clearly, an intrinsic Meissner effect will not be observed for the semiconductor domains. If a semiconducting domain is surrounded by superconducting metal layers (for example in a lamellar colony), then a magnetic field may be expelled from both the metal and semiconductor. The behavior of the bulk alloy must reflect this "shielding" effect.

To simplify the discussion, the following simple model is adopted for the microstructure. Consider a series of alternating layered domains of superconducting metal and a semiconducting phase as shown in Figure 27. Further, let the alloy consist of many of these lamellar colonies randomly oriented with respect to each other. The metal domains and semiconducting domains are characterized by average thickness t_M and t_S, respectively. The magnetic behavior of such a lamellar colony containing superconducting metal domains is now analyzed and compared to the observed behavior of the as-cast Al-Ge alloys. The magnetic behavior of liquid-quenched Al-Si alloys is then treated.

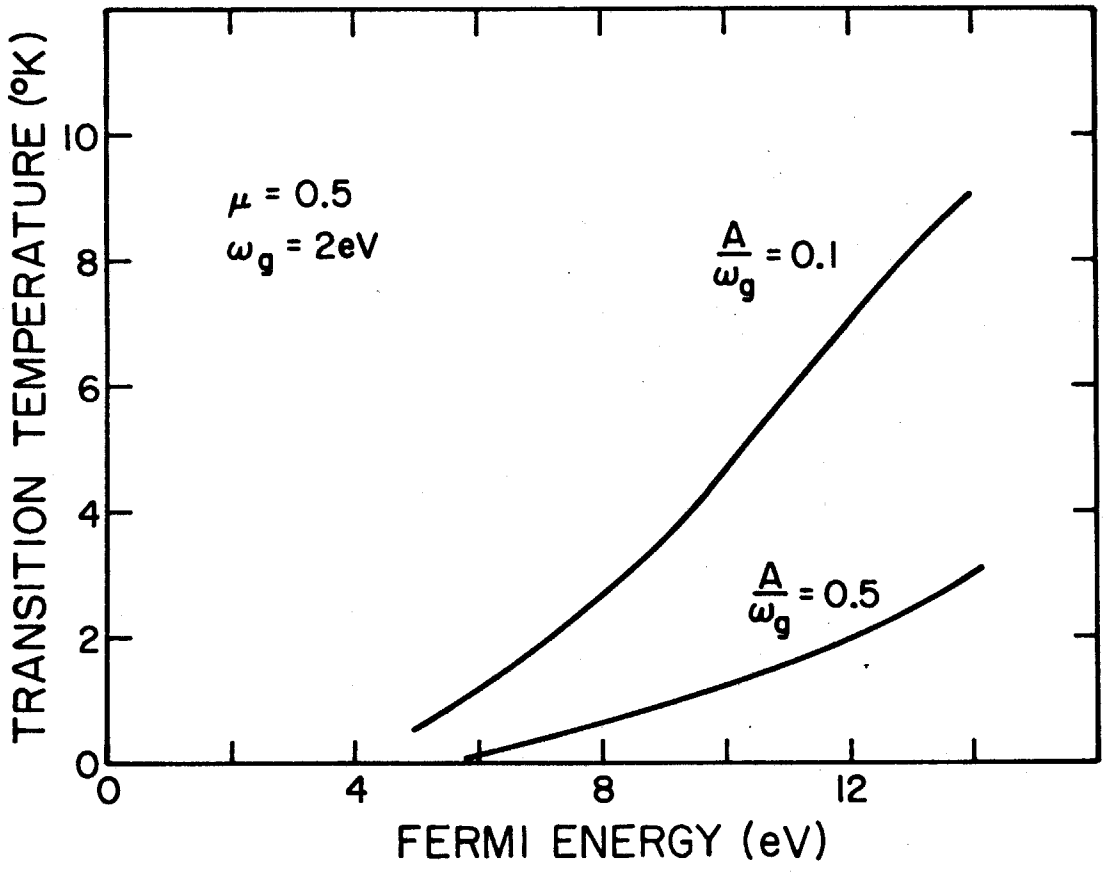

FIGURE 26. Example of Results of Numerical Calculations by ABB Showing the Predicted Dependence of T_c on the Fermi Energy of the Metal. In the Figure, A is the Width of the Exciton Spectrum, and μ is the Coulomb Coupling Constant.

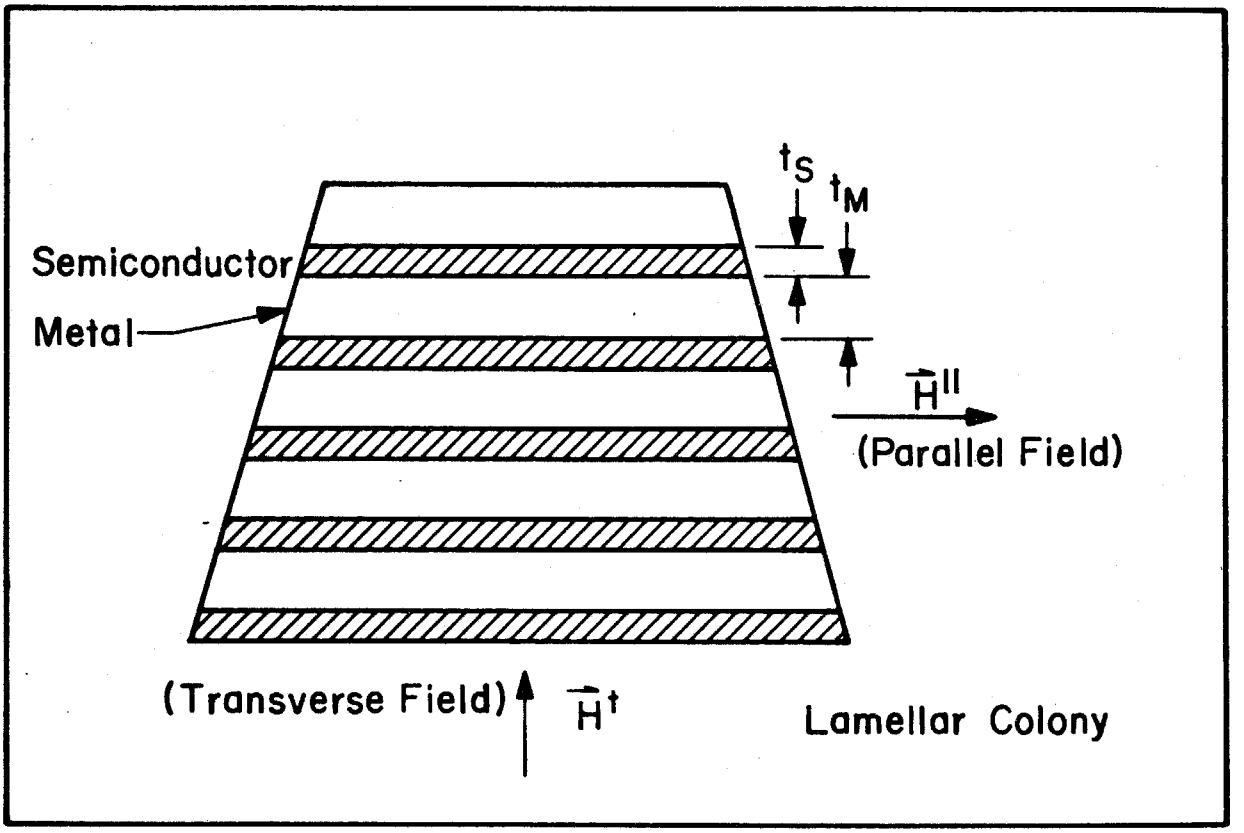

FIGURE 27. Illustration of the Model of a Lamellar Colony Used in Calculating the Magnetic Properties of As-cast $Al_{70}Ge_{30}$.

The thermodynamic critical field for the Al domains in the as-cast $Al_{70}Ge_{30}$ alloy can be estimated using the expression (Reference 41):

$$\frac{H_o^2(0)}{8\pi} = (\tfrac{1}{2})N(E_F)\Delta^2(0) \qquad (10)$$

and the BCS expression for the energy gap $\Delta(0) = 1.75\ k_B T_c$. (Reference 41.) The value $N(E_F) = 1.7 \times 10^{22}$ (states/eVcm^3) is calculated from the free electron approximation assuming a valency of three for Al. The above procedure assumes that the Al domain are homogeneous and can be characterized by a single transition temperature ($T_c = 1.85^oK$). The result is $H_o(0) \cong 160G$. Using $H_c(T) = H_o(0)\ (1 - T/T_c)^2$, (Reference 41) one obtains $H_o(T = 1.3^oK) = 80G$. For a magnetic field oriented transversely to a lamellar colony (see Figure 27), a complete Meissner effect requires that magnetic flux be expelled from both the metal and semiconducting domains. Since $t_M \cong 2t_S$ (see SEM micrograph in Figure 2) this would lead to a reduction in the critical field in the transverse direction. Designating the transverse critical field $H_o^t(T)$, and using the expression

$$t_M\{(\tfrac{1}{2})N(E_F)\Delta^2(0)\} = \frac{(t_M + t_S)\ (H_c^t(0))^2}{8\pi} \qquad (11)$$

which equates the condensation energy of the superconducting domains to the magnetic energy associated with a complete Meissner effect gives $H_o^t(T) = \{t_M/(t_M + t_S)\}^{\frac{1}{2}}\ H_o(T)$. Thus $H_o^t\ (T = 1.3^oK) \cong 65G$. For a magnetic field parallel to the lamellar collony, the critical field

is just $H_o^{||}(T) = H_o(T)$ provided that t_M can be considered to be of macroscopic dimensions. The above argument does not take into account the possibility that type II superconducting behavior may be present, nor the fact that dimensional effects can arise when t_M is small compared to the characteristic fundamental lengths λ (the London penetration depth) and ξ (the coherence length).

The measured magnetization M(H) at T = 1.3°K is shown in Figure 10 for as-cast $Al_{70}Ge_{30}$. M(H) is seen to be linear for H < 35G. For H > 35G, a rapidly decreasing magnetization is observed. The behavior is that of a type II superconductor with $H_{c1}(T = 1.3^oK) \cong 35G$. The magnetoresistivity measurement (Figure 5) indicates that the upper critical field $H_{c2}(T = 1.3^oK) \cong 85G$. Taken together, these results indicate that the superconducting phase can be characterized by a thermodynamic critical field $35G < H_o < 85G$ at T = 1.3°K along with a Ginzburg-Landau parameter $\kappa = \lambda/\xi = (1/\sqrt{2})(H_{c2}/H_o) \gtrsim 1$. (References 42 and 43.) Both the estimated values H_o^t (1.3°K) and $H_o^{||}$ (1.3°K) are within the observed range for H_o (1.3°K). The calculated thermodynamic critical fields are reasonable.

In order to determine whether the above value of κ is reasonable, we must attempt to calculate κ from other intrinsic parameters. Both λ and ξ may be estimated from T_c, l_{mfp}, and n, the density of valence electrons. The electronic mean free path l_{mfp} for the Al domains can be estimated from:

$$l_{mfp} \cong \frac{v_F M}{ne^2\rho_o} \qquad (12)$$

where V_F is the Fermi velocity estimated from the free electron model, M is the electronic mass, and ρ_o is the residual resistivity of the alloy. Taking $\rho_o \sim 5 \times 10^{-5}$ Ωcm measured for $Al_{70}Ge_{30}$ gives $l_{mfp} \sim 10\text{Å}$. This does not take into account the fact that the alloy contains a semiconducting phase. If the resistivity of the lamellar colony in Figure 27 were measured in the parallel direction, the only ∿ 2/3 of the cross-section (the Al phase) would be effective in conduction. The semiconducting phase has negligible conductivity. In the transverse direction, the conductivity is limited by conductivity of the semiconductor. An average of the conductivity over all orientations of the lamellar colony is obtained integrating over all orientations and noticing that the conductivity for a given orientation is given by $\sigma \sim \sigma_M(2/3) \sin^2 \theta$, σ_M = intrinsic conductivity of the Al domains and $\theta = \pi/2$ for the parallel orientation, while $\theta = 0$ for the transverse orientation. This gives:

$$\sigma_{Av} = (2/3)\sigma_M \int_0^1 \sin^2 \theta d(\cos \theta) \qquad (13)$$

$$= 4/9\sigma_M$$

The measured conductivity of the alloy is only ∿ (4/9) the intrinsic conductivity of the Al. The intrinsic mean free path should thus be $l_{mfp} \sim 20\text{Å}$. This is a rough approximation for the effect of the semiconducting phase.

The coherence length of a superconductor in the dirty limit is given by (References 43 and 44):

$$\xi(T) = 0.85\,(\xi_0 l_{mfp})^{\frac{1}{2}}\left(1 - \frac{T}{T_c}\right)^{-\frac{1}{2}} \qquad (14)$$

valid when $l_{mfp} << \xi_0$ and $l_{mfp} << \lambda$. The penetration depth is given by the Pippard formula (References 43 and 44):

$$\lambda(T) = 0.615\left(\frac{3c^2}{8\pi N(E_F)V_F^2 e^2}\right)^{\frac{1}{2}}\left(\frac{\xi_0}{l_{mfp}}\right)^{\frac{1}{2}}\left(1 - \frac{T}{T_c}\right)^{-\frac{1}{2}} \qquad (15)$$

valid when $l_{mfp} << \xi_0$ and $l_{mfp} << \lambda$. In the above formulae, $\xi_0 = \hbar V_F/\pi\Delta(0)$ and $N(E_F)$ and V_F are calculated using the free electron approximation. Taking $l_{mfp} = 20\text{Å}$ for the Al phase in as-cast $Al_{70}Ge_{30}$, and $T_c = 1.85^oK$ gives $\xi(T = 1.3^oK) \cong 860\text{Å}$ and $\lambda(T = 1.3^oK) \cong 1500\text{Å}$. This in turn yields an estimated Ginzburg-Landau parameter $\kappa = \lambda/\xi \cong 1.7$. The measured values of $H_{c1} \cong 35G$ and $H_{c2} \cong 85G$ from Figure 10 and Figure 5 indicate $\kappa \gtrsim 1$. The calculated value is in reasonable agreement considering the rough nature of estimating l_{mfp}. The important fact is that the observed type II behavior can be accounted for in terms of fundamental parameters of the superconductor.

In the as-cast $Al_{70}Ge_{30}$ alloy, the thickness of the Al domains (t_M) ranges down to $\sim 1000\text{Å}$. Since the above estimated coherence length is of the order of 1000Å, surface effects are expected. In particular, surface superconductivity can be expected to persist for a magnetic field oriented parallel to an Al domain when $H > H_{c2}$. The parallel nucleation field for a thin slab is given by (Reference 44):

$$H^{||} = \sqrt{6}\left(\frac{\lambda(T)}{t_M}\right)H_0(T) \qquad (16)$$

Surface superconductivity can persist in the slab for fields $H_{c2} < H < H^{||}$. Since $\lambda \sim 1500A$ ($T = 1.30^{o}K$), it is seen that for $t_M \sim 1000\mathring{A}$, $H^{||}(T = 1.3^{o}K) \sim 3.7 \times H_o(T = 1.3^{o}K)$. Taking the estimated value $H_o(T = 1.3^{o}K) \cong 80G$ gives $H^{||} \sim 300G$. In Figure 5, the persistence of superconductivity up to $H \sim 300G$ is seen. Figure 10 indicates persistence up to even higher fields. This behavior is probably associated with the parallel nucleation field of the Al domains. In summary, the observed magnetic properties of the as-cast $Al_{70}Ge_{30}$ can be accounted for within the framework of the BCS theory together with Ginzburg-Landau formalism. A summary of parameters relevant to the magnetic properties of the alloy is presented in Table VII.

Attention is now given to the case of liquid-quenched Al-Si alloys. Due to the irregular and non-uniform microstructure of the liquid-quenched Al-Si alloys (Figure 3), a description in terms of the simple model of Figure 27 is not appropriate. It is rather difficult to take into account the influence of the Si phase on the magnetic properties. Thus, attention is focused on the intrinsic properties of the superconducting phase.

For liquid-quenched $Al_{70}Si_{30}$ with $T_c = 5.8^{o}K$, we can estimate the thermodynamic critical field using Equation (10). This gives $H_o(0) \cong 500G$ and $H_o(T = 1.3^{o}K) \cong 480G$. The magnetization curve in Figure 16 shows that a complete Meissner effect is observed only for $H \leq 125G$ at $T = 1.4^{o}K$. The magnetoresistivity measured at $T = 1.3^{o}K$ is shown in Figure 14 and shows that the upper critical field is about 3.5kG. The behavior is that of a type II superconductor with

	$Al_{70}Ge_{30}$ (As-cast)	$Al_{70}Si_{30}$ (Liquid-Quenched)
Thermodynamic Critical Field $H_o(T)$ (Calculated)	80G	480G
Lower Critical Field $H_{c1}(T)$ (Observed)	35G	125G
Upper Critical Field $H_{c2}(T)$ (Observed)	85G	3.5×10^3G
Ginzburg-Landau Parameter κ (Calculated)	$1 < \kappa < 1.7$	~ 7.0
Coherence Length $\xi(T)$ (Calculated)	~ 860Å	~ 160-300Å
Penetration Depth $\lambda(T)$ (Calculated)	~ 1500Å	~ 2100Å

TABLE VII. Summary of Parameters Characterizing the Magnetic Properties of As-cast $Al_{70}Ge_{30}$ and Liquid-Quenched $Al_{70}Si_{30}$. The Temperature is Taken to be 1.3^oK for Temperature Dependent Parameters.

$H_{c1}(T = 1.3^{o}K) \simeq 125G$ and $H_{c2}(T = 1.3^{o}K) \simeq 3.5kG$. Using the expression $\kappa = (1/\sqrt{2})(H_{c2}/H_{o})$ and the estimated value of $H_{o} = H_{o}(T = 1.3^{o}K) \simeq 480G$ yields an estimate of $\kappa \sim 7$. From Equations (14) and (15), it can be seen that $\kappa = \lambda/\xi$ is proportional to $(l_{mfp})^{-1}$ and roughly independent of $\Delta(0) = 1.75\ k_{B}T_{c}$. This implies that l_{mfp} is substantially smaller for liquid-quenched $Al_{70}Si_{30}$ than for as-cast $Al_{70}Ge_{30}$. Since only a rough determination of the resistivity of the Al phase was made due to the irregular shape and non-uniform thickness of the liquid-quenched samples, l_{mfp} can only be roughly approximated. Taking $\rho_{o} \simeq 1.5 \times 10^{-4}\Omega cm$ for liquid-quenched $Al_{70}Si_{30}$ (Table III), and using the free electron approximation in Equation (12) with $n = 18.1 \times 10^{22}\ cm^{-3}$ (for Al) gives $l_{mfp} = 3\text{Å}$. Using Equation (14), the coherence length can then be estimated. With $\Delta(0) = 1.75\ k_{B}T_{c}$ and $T_{c} \simeq 5.7^{o}K$, one obtains $\xi(T = 1.4^{o}K) \simeq 160\text{Å}$. The coherence length can be estimated directly from $H_{c2}(T)$ using (Reference 44):

$$\xi(T) = \left(\frac{\Phi_{o}}{2\pi H_{c2}(T)}\right)^{\frac{1}{2}} \qquad (17)$$

where Φ_{o} is the fundamental flux quantum. Using the measured value $H_{c2}(T = 1.4^{o}K) = 3.5kG$ gives $\xi(T = 1.4^{o}K) = 300\text{Å}$. From Equation (14), we can then find l_{mfp} since $\xi_{o} = hV_{F}/\pi\Delta(0)$ can be estimated using the free electron model. This procedure yields an estimate of $l_{mfp} \simeq 5\text{Å}$, which is in reasonable agreement with the estimated value of $l_{mfp} \simeq 3\text{Å}$. Such a short mean free path is consistent with the presence of large concentrations (up to $\sim$ 11 at.%) of dissolved Si in the Al domains as

was discussed in Section III.

In Figure 14 and Figure 16, it can be seen that small amounts of superconductivity persist for $H \lesssim 10$kG. As in the case of as-cast $Al_{70}Ge_{30}$, this can be attributed to the parallel nucleation field of small Al domains situated between Si domains. From the SEM work (Figure 3) it can be seen that Al domains ranging in size down to $t_M \sim 250\text{Å}$ are present. Using $H^{||}(T) = \sqrt{6}\,(\lambda(T)/t_M)H_o(T)$ (Reference 44), $\lambda = \kappa\xi \sim 7 \times (300\text{Å}) = 2100\text{Å}$, and $H_o(T = 1.4^oK) = 480G$, one finds that $t_M \sim 250\text{Å}$ will yield $H^{||}(T = 1.4^oK) \sim 10$kG. This is in good agreement with the observed persistence of superconductivity for fields up to $\sim$ 10kG. A summary of parameters characterizing the magnetic behavior of liquid-quenched $Al_{70}Si_{30}$ is given in Table VII.

C. Size Effects

At this point, it is worthwhile to briefly discuss what is termed the "size effect" observed for thin films. In particular, it is important to compare results obtained for thin films of Al, Be, Sn, Pb, and other soft metals to the results obtained in this study. Thin films of Al obtained by vapor deposition in the 10^{-6} torr range show a significant enhancement of T_c. (References 23 and 39.) A maximum transition temperature of $\sim$ 5-6^oK is obtained for ultrathin films of thickness $\sim$ 30Å deposited on a cryogenic substrate; however, more recent results (Reference 6) for Al films obtained in the 10^{-9} torr range show that no significant enhancement of T_c occurs under these vacuum conditions. For this reason, the enhancement effect has been associated with the presence of oxygen and gaseous contamination. Similar results were

found for Sn films. (Reference 6.) Enhancements up to $\sim 7^{o}K$ are found when films are deposited on cryogenic substrates in a poor vacuum. The enhancement effect for Sn disappears when the vacuum is in the 10^{-9} torr range or better. (Reference 6.) Relatively thick $Al\text{-}Al_2O_3$ films co-deposited at room temperature have transition temperatures above $2^{o}K$. In sum, the enhancement effect for Al films does not result from small sample dimensions alone, but is associated with the presence of oxygen impurities and other gaseous contamination. There is a possibility that the enhancement may have its origin in the excitonic mechanism. On the other hand, the softening of phonon modes can also provide a consistent description of these results. The "size effect" observed in thin films of Be is even more pronounced. Thin Be films have been found to have $T_c \sim 9^{o}K$, and Be films co-deposited with dielectric material have $T_c \sim 11^{o}K$. (Reference 40.) The metal Be readily forms a highly stable oxide BeO, and unless an extremely high vacuum is used ($< 10^{-8}$ torr), the presence of significant amounts of this oxide is unavoidable. Finally, it is extremely interesting to note that very similar enhanced transition temperatures have been observed for Al, Sn, and Be in both the present case and in the case of thin films. For this reason, it seems likely that both effects are related to the same underlying mechanism.

V. SUMMARY AND CONCLUSIONS

The superconducting properties, microstructure, and crystal structure of several metal semiconductor eutectic alloys were investigated in this study. Using the liquid-quenching technique, the characteristic scale of the microstructure was varied. It was demonstrated that the typical domain sizes could be reduced to the order of 100Å for Al-Si alloys when the cooling rate from the liquid state is of the order 10^6 °C/sec. This provides a potentially favorable setting for the observation of effects arising from an interface interaction on the superconductivity of the metallic phase. In particular, it provides a possible setting for the observation of the "excitonic" enhancement of superconductivity proposed by Allender, Bray, and Bardeen. (Reference 2.)

Enhancement of the bulk metal superconducting transition temperature T_{co} was observed in simple eutectic alloys based on the metals Al, Be, Sn, and Pb combined with Ge and Si; whereas no effect was found for the metals In and Tl. The enhancement of T_c was found to depend on the cooling rate from the melt; samples in the as-quenched condition showing the largest effect. Prolonged annealing of the samples above room temperature resulted in the lowering of T_c to the value observed in the as-cast alloys.

Several explanations of the observed enhancement effect were considered. Two of these, the McMillan theory of phonon mode softening, and the ABB model were dealt with in considerable detail. The McMillan

approach yields a consistent account of the observed transition temperatures in Al-Ge and Al-Si alloys. It was suggested that the mean square phonon frequency $\langle\omega^2\rangle_M$ of equilibrium (as-cast and annealed) alloys could be related to the melting temperature of the alloys given in the phase diagram. The Lindemann relation was used to relate the melting temperature to $\langle\omega^2\rangle_M$. Further, it was shown that the phase diagram can be used to obtain the "effective" melting temperature of non-equilibrium alloys. The non-equilibrium (liquid-quenched) alloys are treated by assuming that the terminal solid solubility of Ge and Si in Al is extended by liquid quenching. Changes in $\langle\omega^2\rangle_M$ for the equilibrium solid solution are then extrapolated linearly to obtain values of $\langle\omega^2\rangle_M$ for the metastable solid solutions. This description implies that significant softening of the phonon spectrum can occur without large density changes or the presence of large internal surface area as assumed in previous work on thin films. In addition to accounting for the observed behavior of T_c, this description also explains the observed annealing behavior of the liquid-quenched Al-Si alloys, and the tendency to form metastable crystalline phases in the Al-Ge system. Although a detailed analysis based on the phase diagram was not possible for the Pb-Ge and Sn-Ge alloys, it was shown that the maximum enhancement for these alloys could be predicted from the McMillan approach and agrees well with the observed values of T_c'. Results for the Be-Si alloys can not be easily described in terms of softening of phonon modes. It was suggested that a significant change in the electronic density of states at the Fermi level might occur as a result of disorder introduced by liquid-quenching or the presence of small amounts

of dissolved Si in Be.

The ABB model was used to evaluate the possible role of an interface interaction in the enhanced superconductivity of the metals. Although a consistent description of the enhancement effect in Al-Si and Al-Ge can be given, it involves several experimentally inaccessible parameters. An interesting relation between the Fermi energy of the metals calculated using the free electron model, and the maximum observed enhancement of T_c was pointed out. Metals having the highest density of free electrons show the greatest increase in T_c. This relation is consistent with the ABB model.

In addition to the discussion of the transition temperature, it was shown that the magnetic behavior observed for the alloys could be explained within the framework of the Ginzburg-Landau theory of type I and type II superconductors. The thermodynamic critical field H_o observed is consistent with the BCS relations $\Delta = 1.75\ k_B T_c$, and $H_o^2 = 4\pi N(E_F)\Delta^2$ where the electronic density of states at the Fermi level is calculated using the free electron model. The large increase in the upper crticial field H_{c2} of the liquid-quenched alloys as compared to that of the as-cast alloys can be simply understood in terms of the reduction in the electronic mean free path. In summary, there are no indications of unusual behavior in the magnetic properties of the alloys.

Recently several criticisms of the ABB model have been made (Reference 45). The fact that several experimentally inaccessible parameters are involved in applying the ABB model to the present results make this interpretation rather doubtful. In view of the

simpler consistent description of the results in terms of the McMillan approach, it seems at present unnecessary to invoke the ABB model to explain them. Unless further evidence is found, it must be concluded that the case for "excitonic superconductivity" is not very convincing in the present study.

REFERENCES

1. V. L. Ginzburg, Contemp. Phys. 9, 355 (1968); Sov. Phys. Usp. 13, 355 (1970); Zh. Eksp. Teor. Fiz. Pis'ma Red. 14, 572 (1971) {JETP Lett. 14, 396 (1971)}.

2. D. Allender, J. Bray, and J. Bardeen, Phys. Rev. B 7, 1020 (1973).

3. J. P. Hurault, J. Bray, and J. Bardeen, Phys. Rev. B 7, 1020 (1973).

4. W. A. Little, Phys. Rev. A 34, 1416 (1964).

5. L. N. Bulaeskii and Y. A. Kukharenco, Zh. Eksp. Teor. Fiz. 60, 1518 (1971) {Sov. Phys. JETP 33, 821 (1971)}.

6. M. Strongin, O. F. Kammerer, and H. H. Farrell, Phys. Rev. Lett. 30, 129 (1973).

7. A. Fontaine and F. Meunier, Phys. Kondens. Mater. 14, 119 (1972).

8. M. Strongin, O. F. Kammerer, and H. H. Farrell, Phys. Rev. Lett. 21, 132 (1968).

9. M. Hansen, Constitution of Binary Alloys, (McGraw-Hill, New York, 1958).

10. P. Duwez, Trans. Quarterly ASM 60, 605 (1967).

11. W. B. Pearson, Handbook of Lattice Spacings and Crystal Structure of Metals, (Permagon Press, New York, 1967).

12. A. Hellawell, Trans. AIME 239, 1049 (1967).

13. G. A. Chadwick, Liquids; Structure Properties, Solid Interactions, edited by T. J. Hughel (Elsevier, Amsterdam, 1965), p. 327.

14. Previous attempts to obtain new metastable phases by liquid-quenching Al-Si alloys have been unsuccessful. {C. Suryanarayana, Scr. Mettal. 5, 337 (1971)}.

15. M. Itagaki, B. Giessen, and N. J. Grant, Trans. Am. Soc. Met. 61, 330 (1968).

16. C. Suryanarayana and T. R. Anatharaman, J. Mat. Sci. 5, 992 (1970).

17. P. Ramachandrarao, M. G. Scott, and G. A. Chadwick, Philos. Mag. 25, 961 (1972).

18. V. N. Bogomolov et al., Fiz. Tverd. Tela 11, 3648 (1969) {Sov. Phys. Solid State 11, 3064 (1970)}.

19. W. L. McMillan, Phys. Rev. 167, 331 (1968).

20. M. Strongin, O. F. Kammerer, J. E. Crow, R. D. Parks, D. H. Douglass, and M. A. Jensen, Phys. Rev. Letters 21, 1320 (1968).

21. V. L. Ginzburg and D. A. Kirzhnits, J. Exptl. Theor. Phys. (U.S.S.R.) 46, 397 (1964).

22. J. S. Faulkner, Phys. Rev. 178, 914 (1969).

23. M. Strongin, Physica 55, 155 (1971).

24. J. M. Dickey and A. Paskin, Phys. Rev. Lett. 21, 441 (1968).

25. J. J. Hauser, Phys. Rev. B 3, 1611 (1971).

26. J. Klein and A. Leger, Phys. Letters 28A, 134 (1968).

27. W. L. Johnson and S. J. Poon (to be published).

28. G. Deutscher, J. P. Farges, F. Meunier, and P. Nedellec, Physics Letters 35A, 265 (1971).

29. F. A. Lindemann, Z. Physik 11, 609 (1910).

30. D. Kulmann-Wilsdorf, Physical Review 140, A1599 (1965).

31. A. W. Klement, Trans. Metall. Soc. AIME 233, 1180 (1965).

32. T. R. Anantharaman and C. Suryararyana, J. Mater. Sci. 6, 1111 (1972).

33. R. P. Elliot, Constitution of Binary Alloys - First Supplement, (McGraw-Hill, New York, 1965).

34. F. A. Shunk, Constitution of Binary Alloys- Second Supplement (McGraw-Hill, New York, 1969).

35. W. Hume-Rothery, Elements of Structural Metallurgy, Monograph No. 26, Institute of Metals, London (1961).

36. E. Bucher, F. Heiniger, J. Muller, P. Spitzli, Phys. Letters 19, 263 (1965).

37. M. Strongin, O. F. Kammerer, J. Crow, R. S. Thompson, H. L. Fine, Phys. Rev. Lett. 20, 922 (1968).

38. R. E. Glover, Phys. Letters 25A, 542 (1967).

39. B. Abeles, R. W. Cohen, and G. W. Cullen, Phys. Rev. Lett. 14, 949 (1965).

40. N. E. Alekseevski, V. I. Tsebro, and E. I. Fillippovich, Zh. Eksp. Teor. Fiz. Pis'ma Red. 13 , 247 (1971) {JETP Lett. 13, 174 (1971)}

41. J. Bardeen, L. N. Cooper, and J. R. Schrieffer, Phys. Rev. 108, 1175 (1957).

42. V. L. Ginzburg and L. D. Landau, Zh. Eksperim. i Tear. Fiz. 20, 1064 (1950).

43. D. Saint-James, E. J. Thomas, G. Sarma, Type II Superconductivity (Permagon Press, New York, 1969).

44. P. G. De Gennes, Superconductivity of Metals and Alloys (W. A. Benjamin Inc., New York, 1966).

45. J. C. Inkson, P. W. Anderson, Phys. Rev. B8, 4429 (1973).